

# Context-aware Constrained Reinforcement Learning Based Energy-Efficient Power Scheduling for Non-stationary XR Data Traffic

Kexuan Wang and An Liu, *Senior Member, IEEE*

**Abstract**—In XR downlink transmission, energy-efficient power scheduling (EEPS) is essential for conserving power resource while delivering large data packets within hard-latency constraints. Traditional constrained reinforcement learning (CRL) algorithms show promise in EEPS but still struggle with non-convex stochastic constraints, non-stationary data traffic, and sparse delayed packet dropout feedback (rewards) in XR. To overcome these challenges, this paper models the EEPS in XR as a dynamic parameter-constrained Markov decision process (DP-CMDP) with a varying transition function linked to the non-stationary data traffic and solves it by a proposed context-aware constrained reinforcement learning (CACRL) algorithm, which consists of a context inference (CI) module and a CRL module. The CI module trains an encoder and multiple potential networks to characterize the current transition function and reshape the packet dropout rewards according to the context, transforming the original DP-CMDP into a general CMDP with immediate dense rewards. The CRL module employs a policy network to make EEPS decisions under this CMDP and optimizes the policy using a constrained stochastic successive convex approximation (CSSCA) method, which is better suited for non-convex stochastic constraints. Finally, theoretical analyses provide deep insights into the CDAC algorithm, while extensive simulations demonstrate that it outperforms advanced baselines in both power conservation and satisfying packet dropout constraints.

**Index Terms**—Extended reality, power scheduling, constrained reinforcement learning, non-stationary data traffic.

## I. INTRODUCTION

Extended reality (XR) represents a category of emerging applications in sixth-generation (6G) communications, characterized by orders of magnitude larger packets than those in traditional low-latency applications such as the Internet of Things (IoT) and Vehicle-to-Everything (V2X) [1]. Considering the latency-sensitive nature of users, XR applications require each data packet must be successfully transmitted within a *hard*-latency constraint; otherwise, the packet will be discarded [2]. Moreover, meeting this stringent requirement often demands significant transmitting power resources, which can lead to unaffordable economic costs and environmental crises [3]. As a result, developing advanced energy-efficient power scheduling (EEPS) algorithms to support XR has become a critical research topic, attracting widespread attention from both academia and industry [4], [5].

Previous research efforts have extensively investigated low-latency EEPS and other radio resource scheduling (RRS) [6]–[8], however, most of them focused on reducing the average queue backlog (*soft*-latency constraint), which cannot avoid

packet dropouts in XR transmission. Only a few algorithms [9]–[12] considered hard-latency constraints, and they still focused on designing heuristics for a specific environment model. For example, [9] simply scheduled the packet closer to its deadline on a good channel condition; a heuristic non-causal packet scheduler was used for the causal case in [10]; analyses in [11] and [12] were limited to AWGN channels and Poisson-distributed packet arrival process, respectively. These traditional methods often lead to poor performance and generalization ability in the real world. Recently, [13] modeled the RRS problem as a constrained Markov Decision Process (CMDP) and solved it by a constrained deep Actor-Critic (CDAC) algorithm, which belongs to a category of advanced constrained reinforcement learning (CRL) algorithms. Without any prior information, CDAC [13]–[15] learns the environmental model information in a model-free manner and optimize a policy for making decisions online, achieving satisfactory simulated performance in RRS and many other sequential decision-making problems, which greatly inspires this paper. However, the existing CDAC algorithms are still in need of further development to be applied to EEPS/other RRS tasks in downlink XR transmission.

Modern CDAC algorithms usually employ deep neural networks (DNNs) to avoid the curse of dimensionality in practical sequential decision tasks with large continuous state and action space [14]. This approach introduces non-convexity into both the objective function and the constraints of CRL problems [6]. Unfortunately, most existing CDAC algorithms can only handle problems with simple convex constraints. Specifically, there are two major categories of policy optimization methods in existing CDAC algorithms [6]: primal-dual methods [15]–[19] and CPO [20]–[22]. The primal-dual methods, represented by trust region policy optimization-Lagrangian (TRPO-Lag) and proximal policy optimization-Lagrangian (PPO-Lag) [15], casts the original problem into an unconstrained max-min saddle-point problem and searches for optimal policies in the primal-dual domain. Although [23] proved that a general class of CRL problems can be solved exactly in the convex dual domain, the method of performing the non-convex optimization in the primal domain is still open. Most existing primal-dual methods simply adopt the stochastic gradient descent (SGD) method to update policy [15]–[17], which makes them only suitable for simple constraints where the feasible set can be represented by a deterministic convex set. Although authors in [18] and [19] applied optimistic gradient descent methods to accelerate convergence, they still allowed the agent to violate the safety constraints by oscillating around an optimal safety policy. Authors in [20]–[22]

Kexuan Wang and An Liu are with the College of Information Science and Electronic Engineering, Zhejiang University, Hangzhou 310027, China (email: {kexuanWang, anliu}@zju.edu.cn). (*Corresponding Author: An Liu*)

proposed the constrained policy optimization (CPO) algorithm, which updates the policy within a trust-region framework. Nevertheless, due to the non-convexity and high computation complexity, the CPO introduces some approximate operations at the cost of sacrificing the stable performance [22] and also cannot assure a feasible final result. In particular, our previous work [6] considered non-convexity in the algorithm design, however, it simply adopted the Monte Carlo (MC) method to estimate Q values and belongs to the Actor-only algorithm, which suffers from a slow convergence.

Moreover, the non-stationary data traffic (packet arrival dynamics) and sparse delayed feedback (rewards) for packet dropouts in downlink XR transmission can also pose serious challenges to the existing CDAC algorithms, which however, are generally ignored. Specifically, conventional CDAC algorithms typically assume that the environment dynamics are stationary [24]. However, in XR scenarios, the packet arrival probabilities and distributions of packet lengths continuously change due to their close relationship with the type of each user's online activities and the peak and off-peak hours [25]. As a result, conventional CDAC algorithms must learn the environmental model information from scratch whenever the packet arrival dynamics undergo changes, which may require a long adaptation time. Meta-learning is a category of methods that can enhance the adaptability of machine learning (ML) algorithms in various tasks/dynamic environments, divided into gradient-based meta-learning and context-based meta-learning [26]. The gradient-based methods [26]–[28] attempt to learn effective initial parameters by exploring the common structures of various tasks/environment dynamics, thereby reducing the convergence time of the algorithms. The context-aware methods [29]–[31] encode the features of each task/environment dynamic into a specific latent variable to guide ML algorithms towards faster convergence. Because hidden variables can represent both similarities and differences between different environmental dynamics, context-aware methods tend to be better suited to a rapidly changing environment than gradient-based methods [30]. An initial exploration to bridge a typical gradient-based meta-learning method, i.e., MAML, into CPO is made in [27]. However, to the best of our knowledge, the context-aware meta-learning enabled CDAC in a non-stationary environment has not been investigated. In addition, because the sparse rewards for packet dropouts can only be received when the hard-latency constraints are reached, the existing methods all tend to be inefficient or fail in XR transmission, which makes the problem even trickier.

To combat these challenges above, this paper brings up a context-aware constrained reinforcement learning (CACRL) algorithm to support the energy-efficient power scheduling (EEPS) task in XR downlink transmission with non-stationary XR data traffic. Note that this algorithm is also easy to extend to scheduling other radio resources with trivial modifications. The main contributions are as follows:

- **More realistic and tractable problem formulation:** We formulate the EEPS task in XR downlink transmission as a dynamic parameter-constrained Markov Decision Process (DP-CMDP). By using long-term power consumption and packet dropout rates as performance

metrics, the DP-CMDP formulates the requirements of XR applications appropriately. Moreover, by adopting a transition distribution defined by dynamic parameters, the DP-CMDP can model the non-stationary nature of XR data traffic, a feature overlooked in the general CMDP.

- **An advanced CACRL Algorithm:** We propose an advanced CACRL algorithm consisting of a context inference (CI) module and a CRL module to address the challenging DP-CMDP. Specifically, by integrating a context-aware meta-learning method and a potential-based reward reshaping method, the CI module utilizes an encoder to characterize the current transition function according to recent observation samples (which is the so-called context), and employs potential networks to transform the original packet dropout rewards into dense immediate ones. These operations transform the original DP-CMDP problem into a general CMDP problem. The CRL module then employs a stochastic policy network to make EEPS decisions under this CMDP and, to better satisfy non-convex stochastic constraints, optimizes the policy using a constrained stochastic successive convex approximation (CSSCA) method, whose main idea is to transform the original non-convex stochastic constraint problem into a series of convex surrogate objectives and feasible optimization problems. Note that the networks in both modules are jointly optimized in model-free manners, without requiring any prior knowledge of the environment model. Special designs are also adopted to minimize the training overhead as much as possible.
- **Theoretical and simulation analyses:** Comprehensive theoretical analyses are provided to offer deep insights into the convergence of the proposed CACRL algorithm. Moreover, sufficient ablation and comparative simulation results further validate the effectiveness of the CI module and the CRL module, demonstrating that the proposed algorithm outperforms advanced baselines both in power conservation and meeting packet dropout constraints.

## II. SYSTEM MODEL AND PROBLEM FORMULATION

### A. System Model

We consider downlink transmission from an  $M$ -antennas base station (BS) to  $K$  single-antenna XR users, as illustrated in Fig. 1. At the BS, each user  $k$  is assigned a separate buffer  $k$ . Data packets from some higher-layer applications randomly arrive at the buffers and are stored in the form of queues. At the same time, the BS dynamically schedules the transmission power resource for the downlink transmission of each data queue. In the following, we provide further details of the data queue model and the downlink transmission process.

1) *Data Queues Model:* In this subsection, we describe the dynamic characteristics of the data queues. We divide time into some  $\tau_0$ s-timeslots and assume that the packet  $X_{k,t}$  of length  $b_{k,t}$  for the  $k$ -th user arrives from upper-layer applications to the BS with a probability  $P_k \in (0, 1)$  at the  $t$ -th timeslot. Note  $P_{k,t}$  and the distribution of  $b_{k,t}$  are typically unknown to the BS. Moreover, since the packet arrival processes are closely related to the frequently switching active users and their

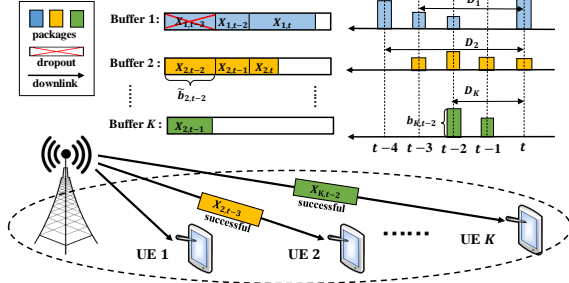


Figure 1. System model and timeslot diagram

ongoing online activities, we assume that potential changes may occur in  $P_{k,t}$  and the distribution of  $b_{k,t}$  at each timeslot  $t$ . The frequency of changes depends on the specific scenario.

The arrived data packets are served according to a first-come-first-served protocol. Considering the latency-sensitive nature of XR users, each packet  $X_{k,t}$  is assigned a *hard*-latency constraint  $D_k$ , i.e., all data packets  $\{X_{k,t-t_d}\}_{t_d=D_k, D_k+1, \dots}$  have been successfully transmitted or dropout. Denoting the remaining length of packet  $X_{k,t}$  as  $\bar{b}_{k,t}$ , we use a binary function  $\mathbb{I}_{k,t}$  to indicate whether a packet dropout occurs at the buffer  $k$  at timeslot  $t$ :

$$\mathbb{I}_{k,t}^{\text{drop}} \triangleq \begin{cases} 1, & \text{if } \bar{b}_{k,t-D_k} > \tau_0 \mathcal{R}_{k,t-1}, \forall k, t \\ 0, & \text{otherwise,} \end{cases}$$

where  $\mathcal{R}_{k,t}$  denotes the transmission rate assigned to buffer  $k$  at timeslot  $t$ . Both transmission power shortage and bad channel conditions can lead to the occurrences of packet dropout. For ease of understanding, we show a possible state of the data queues in Fig. 1.

2) *Downlink Transmission Process*: At each timeslot  $t$ , the downlink channel state information (CSI) matrix is denoted as  $\mathbf{H}_t \triangleq [\mathbf{h}_{1,t}; \mathbf{h}_{2,t}; \dots; \mathbf{h}_{K,t}] \in \mathbb{C}^{K \times M_t}$ , where  $\mathbf{h}_{k,t} \in \mathbb{R}^{1 \times M}$  represents the channel from the BS to the  $k$ -th user. It is assumed that  $\mathbf{H}_t$  is block flat fading. For convenience, we also denote a queue state information (QSI) matrix  $\mathbf{B}_t \in \mathbb{R}^{2 \times \sum_{k=1}^K D_k} \triangleq [\mathbf{b}_{1,t}, \dots, \mathbf{b}_{K,t}; \bar{\mathbf{b}}_{1,t}, \dots, \bar{\mathbf{b}}_{K,t}]$ , where vectors  $\mathbf{b}_{k,t} \in \mathbb{R}^{1 \times D_k} \triangleq [b_{k,t}, \dots, b_{k,t-D_k+1}]$  and  $\bar{\mathbf{b}}_{k,t} \in \mathbb{R}^{1 \times D_k} \triangleq [\bar{b}_{k,t}, \dots, \bar{b}_{k,t-D_k+1}]$  record the original lengths and remaining lengths of packets  $\{X_{k,t-t_d}\}_{t_d=0,1,\dots,D_k-1}$ , respectively.

According to the current CSI  $\mathbf{H}_t$  and QSI  $\mathbf{B}_t$ , the BS schedules power  $p_{k,t}$  for user  $k, \forall k$  for downlink transmission, where we denote  $\mathbf{p}_t \triangleq [p_{1,t}, p_{2,t}, \dots, p_{K,t}] \in \mathbb{R}^{1 \times K}$ . Then, the transmit signal  $\mathbf{x}_t \in \mathbb{C}^{K \times 1} \triangleq [x_{1,t}, x_{2,t}, \dots, x_{K,t}]^T$  satisfying  $\mathbb{E}[\mathbf{x}_t \mathbf{x}_t^H] = \text{Diag}(\mathbf{p}_t)$  is processed by precoding matrix  $\mathbf{V}_t \in \mathbb{C}^{M_t \times L} \triangleq [\mathbf{v}_{1,t}, \mathbf{v}_{2,t}, \dots, \mathbf{v}_{K,t}]$ . Further, we calculate  $\mathbf{V}_t$  by the normalized regularized zero-forcing (RZF):

$$\mathbf{V}_t = \mathbf{H}_t^H (\mathbf{H}_t \mathbf{H}_t^H + \epsilon_t \mathbf{I})^{-1} \mathbf{\Lambda}^{1/2}, \forall t,$$

where  $\mathbf{\Lambda}^{1/2} = \text{Diag}([\|\bar{\mathbf{v}}_{1,t}\|^{-1}, \|\bar{\mathbf{v}}_{2,t}\|^{-1}, \dots, \|\bar{\mathbf{v}}_{K,t}\|^{-1}])$  is the normalization matrix,  $\bar{\mathbf{v}}_{k,t}$  is the  $l$ -th column of  $\bar{\mathbf{V}}_t \triangleq \mathbf{H}_t^H (\mathbf{H}_t \mathbf{H}_t^H + \epsilon_t \mathbf{I})^{-1}$ , and  $\epsilon_t$  is the regularization factor. Note that the RZF precoder is widely used in practical systems and is asymptotically optimal for large  $M_t$  and/or high SNR [32].

Further, the received signal  $y_{k,t} \in \mathbb{C}$  is given by

$$y_{k,t} = \mathbf{h}_{k,t} \mathbf{v}_{k,t} x_{k,t} + \sum_{m \neq k}^K \mathbf{h}_{k,t} \mathbf{v}_{m,t} x_{m,t} + n_l, \forall t, l,$$

where  $n_k \sim \mathcal{CN}(0, \sigma_k^2)$  represents the additive white Gaussian noise. Finally, the transmission rate  $\mathcal{R}_{k,t}$  is given by

$$\mathcal{R}_{k,t} = W \log_2 \left( 1 + \frac{p_{k,t} |(\mathbf{h}_{k,t})^H \mathbf{v}_{k,t}|^2}{\sum_{m \neq k} p_{m,t} |(\mathbf{h}_{k,t})^H \mathbf{v}_{m,t}|^2 + \sigma_k^2} \right), \forall k, t$$

where  $W$  denotes the bandwidth.

## B. Problem Formulation

Considering the characteristics and requirements of XR applications, we model the EEPs task as a dynamic parameter-constrained Markov decision process (DP-CMDP), which can be denoted as a sequence of tuples  $\{\mathcal{M}^{z_t} = (\mathcal{S}, \mathcal{A}, P_T^{z_t}, R, C)\}_{t=0,1,\dots}$  with the following definitions:

- **The state space  $\mathcal{S}$** : the QSI space and CSI space constitute the state space  $\mathcal{S}$ , i.e.,  $\mathbf{s}_t \triangleq \{\text{vec}(\mathbf{B}_t)^T, \text{vec}(\mathbf{H}_t)^T\}$ .
- **The action space  $\mathcal{A}$** : the action consists of the scheduling decision and the regularization factor, i.e.,  $\mathbf{a}_t \triangleq \{\mathbf{p}_t, \epsilon_t\} \in \mathcal{A}$ . Specifically,  $\mathbf{a}_t$  is sampled according to a stochastic policy  $\pi$ . To overcome the curse of dimension, the policy  $\pi$  is parameterized by network  $\pi_\theta$  with  $n_\theta$ -dimensional parameter  $\theta \in \Theta$ .
- **The dynamic transition function  $P_T^{z_t}$** : at each timeslot  $t$ , the transition function  $P_T^{z_t}$  is defined by a latent variable  $\mathbf{z}_t$ , where  $\mathbf{z}_t \in \mathcal{Z}$  is unobservable and determined by the current underlying packet arrival dynamics. The value  $P_T^{z_t}(\mathbf{s}_{t+1} | \mathbf{s}_t, \mathbf{a}_t)$  denotes the probability of transition from  $\mathbf{s}_t$  to  $\mathbf{s}_{t+1}$  upon taking  $\mathbf{a}_t$ . Considering the non-stationary nature of XR data traffic, we assume that  $\mathbf{z}_t$  shifts stochastically according to an unknown distribution  $P_{\text{shift}}(\mathbf{z}_t | \mathbf{z}_{t-1})$ , where  $\mathbf{z}_t \neq \mathbf{z}_{t-1}$  indicates that packet arrival dynamics have changed. Consequently, the sequence  $\{\mathbf{z}_t\}_{t=0,1,\dots}$  is a Markov random process.
- **The reward  $R$  and  $C$** : we define reward functions  $R(\mathbf{s}_t, \mathbf{a}_t) \triangleq \sum_{k=1}^K p_{k,t}$  and  $C_k(\mathbf{s}_t, \mathbf{a}_t) \triangleq \mathbb{I}_{k,t}^{\text{drop}}$ , which respectively represent the transmission power consumption and the number of packet dropouts of each user at the  $t$ -th timeslot. Please note that since the occurrences of packet dropouts are only known when the hard-latency constraints are reached, rewards  $C$  are *sparse* and *delayed*, i.e.,  $\{C_k(\mathbf{s}_t, \mathbf{a}_t)\}_{t=0,1,\dots, \forall k}$ , is a 01 sequence with relatively fewer occurrences of 1.

Note that if  $\mathbf{z}_t$  is known at each timeslot  $t$ , the original DP-CMDP can be transformed into a stationary CMDP  $\mathcal{M} \triangleq (\dot{\mathcal{S}}, \mathcal{A}, P_T, R, C)$  by defining an augmented state space  $\dot{\mathcal{S}} \triangleq \mathcal{S} \times \mathcal{Z}$ , where the transition function  $P_T$  remain unchanged, with the probability  $P_T(\dot{\mathbf{s}}_{t+1} | \dot{\mathbf{s}}_t, \mathbf{a}_t) = P_T^{z_t}(\mathbf{s}_{t+1} | \mathbf{s}_t, \mathbf{a}_t) P_{\text{shift}}(\mathbf{z}_{t+1} | \mathbf{z}_t)$ .

This paper aims to design an algorithm that can, on the one hand, continuously infer  $\{\mathbf{z}_t\}_{t=0,1,2,\dots}$ , and on the other hand, obtain a policy  $\pi_\theta$ , where  $\pi_\theta(\mathbf{a}_t | \dot{\mathbf{s}}_t)$  represents the probability of sampling the action  $\mathbf{a}_t$  given the augmented

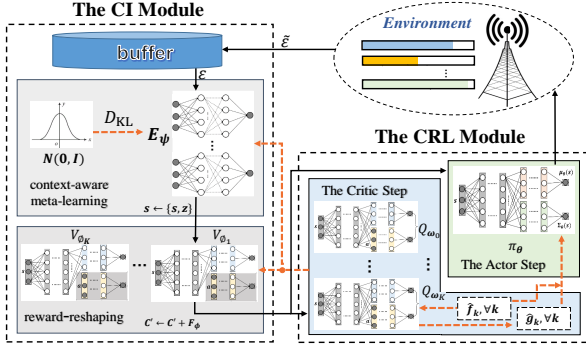


Figure 2. The algorithmic framework of the proposed CACRL, where the black line represents the flow for making EEPs decisions online, and the orange line represents the flow for network training.

state  $\hat{s}_t = \{s_t, z_t\}$ , by solving the following non-convex stochastic optimization problem under the transformed CMDP:

$$\begin{aligned} \min_{\theta \in \Theta} f_0(\theta) &\triangleq \lim_{T \rightarrow \infty} \mathbb{E} \left[ \sum_{t=0}^{T-1} C'_0(s_t, a_t) \right] \\ \text{s.t. } f_k(\theta) &\triangleq \lim_{T \rightarrow \infty} \mathbb{E} \left[ \frac{1}{T} \sum_{t=0}^{T-1} C'_k(s_t, a_t) \right] \leq 0, \forall k, \end{aligned} \quad (1)$$

where we denote  $C'_0(s_t, a_t) = -R(s_t, a_t)$  and  $C'_k(s_t, a_t) = C_k(s_t, a_t) - c_k$  with  $c_k$  representing the allowed maximum packet dropout rate for user  $k$ . The notation  $\mathbb{E}[\cdot]$  denotes the expectation taken over  $\hat{s}_{t+1} \sim P_T(\hat{s}_{t+1} | \hat{s}_t, a_t)$  and  $a_t \sim \pi_\theta(a_t | \hat{s}_{t+1})$ . The goal of problem (1) is to minimize long-term average power consumption while ensuring that the packet dropout rate for each user  $k$  does not exceed  $c_k$ .

*Remark 1.* However, designing such an algorithm is non-trivial. The main reasons are as follows: 1) most existing algorithms are designed for a stationary CMDP without considering the non-stationary nature of the real-world scenarios. Therefore, methods that can effectively infer the latent variables are still lacking, especially in XR scenarios with sparse delayed feedback rewards  $\{C_k(s_t, a_t)\}_{t=1,2,\dots,\forall k}$ ; 2) even if the latent variables can be obtained, it is quite challenging for an algorithm to ensure that the non-convex stochastic constraints are satisfied at a limiting point.

### III. THE CONTEXT-AWARE CONSTRAINED REINFORCEMENT LEARNING ALGORITHM

#### A. Outline of the CACRL Algorithm

To overcome the challenges in Remark 1, this section proposes a CACRL algorithm, which consists of a CI module and a CRL module, as illustrated in Fig. 2.

The CI module integrates a context-aware meta-learning method and a reward-resaping method to infer  $\{z_t\}_{t=0,1,\dots}$  and convert the original packet dropout rewards into immediate dense ones, respectively. Specifically, following the context-aware meta-learning method in [31], we assume that the latent variable  $z_t$  can be inferred from the most recent  $N$  ( $N \leq B$ ) transition tuples  $\tau_t = \{\tilde{\tau}_{t'} \triangleq (s_{t'}, a_{t'}, s_{t'+1})\}_{t'=t-N+1:t}$  (which is the so-called *context*) and train an encoder network for this inference. Once  $z_t$  is obtained, it is embed into  $s_t$  by

$$\hat{s}_t \leftarrow \{s_t, z_t\}, \quad (2)$$

where note that although the latent variable in (2) is merely an estimate of its true value obtained through the encoder network, we still denote it as  $z_t$  for notational simplicity. Differing from [31], the encoder network in this paper is trained jointly with the CRL module in a model-free manner, without relying on any actual or estimated knowledge of the environment model, as elaborated in section III-C. Since the training of the CRL module depends on reward signals  $\{C_k(s_t, a_t)\}_{t=0,1,\dots,\forall k}$ , sparse and delayed rewards could cause slow convergence or even failure in these two modules. To overcome this challenge, the CI module also trains some potential networks to construct a set of reward-resaping functions  $\{F_{\phi_k}\}_{k=1:K}$  and then transform the original packet dropout rewards into dense immediate ones by

$$\dot{C}'_k(\hat{s}_t, a_t, \hat{s}_{t+1}) \leftarrow C'_k(s_t, a_t) + F_{\phi_{k,t}}(\hat{s}_t, \hat{s}_{t+1}), \forall k, t, \quad (3)$$

where we abbreviate  $\dot{C}'_{k,t}$  for  $\dot{C}'_k(\hat{s}_t, a_t, \hat{s}_{t+1})$  in the following. In this way, effective optimizations can be performed without waiting for the arrival of packet dropout rewards.

In the CRL module,  $\pi_\theta$  is chosen as the commonly used Gaussian policy [33], whose mean and variance are output by DNNs  $\mu_{\theta_\mu}$  and  $\Sigma_{\theta_\sigma}$ , respectively, where the parameter  $\theta = [\theta_\mu, \theta_\sigma] \in \Theta$ . In particular, to better handle non-convex stochastic constraints, this paper employs a CSSCA-based policy optimization method. By employing an Actor-Critic framework, the CRL module estimates the objective/constraint values and gradients in (1) at the Critic step and further, uses these estimates to construct a sequence of convex surrogate problems at the Actor step. Then, the CSSCA-based policy optimization method is executed once every  $B$  ( $N \leq B$ ) timeslots, to tackle the original problem (1) by solving the sequence of surrogate problems. After the  $i$ -th update, we obtain an observation set  $\varepsilon_i = \{\tilde{\varepsilon}_t\}_{t=Bi-B+1:Bi}$ , where  $\tilde{\varepsilon}_t \triangleq \{\hat{s}_t, a_t, \{\dot{C}'_{k,t}\}_{k=0,\dots,K}, \hat{s}_{t+1}\}$ , by interacting with the environment using  $\pi_{\theta_i}$ , and store it in a buffer. Note that the tuple  $\tilde{\tau}_t$  in the CI module can be extracted from  $\tilde{\varepsilon}_t$ .

In practice, we treat the first  $I$  iterations as pretraining for the algorithm, and with the pretraining, the algorithm can work effectively with the fine-tuned network at the deployment stage (after the  $I$ -th iteration). Finally, the design details are provided below, and the overall algorithm is summarized in Algorithm 1.

#### B. The CRL Module

1) *The Actor Step Adopting CSSCA-based Policy Optimization:* At the  $i$ -th iteration, the CSSCA method replace the objective/constraint functions  $f_k(\theta)$  by the following convex quadratic surrogate functions based on  $\theta_i$ :

$$\bar{f}_{k,i}(\theta) = \hat{f}_{k,i} + (\hat{g}_{k,i})^\top (\theta - \theta_i) + \zeta_k \|\theta - \theta_i\|_2^2, \forall k \quad (4)$$

where  $\hat{f}_{k,i} \in \mathbb{R}$  and  $\hat{g}_{k,i} \in \mathbb{R}^{n_\theta}$  are the estimations of  $f_k(\theta)$  and  $\nabla f_k(\theta)$ , and  $\zeta_k$  is a positive constant.

Then, based on these surrogate functions, the following objective update problem is first solved:

$$\bar{\theta}_i = \underset{\theta \in \Theta}{\operatorname{argmin}} \bar{f}_{0,i}(\theta) \quad \text{s.t. } \bar{f}_{k,i}(\theta) \leq 0, \forall k. \quad (5)$$

---

**Algorithm 1** The Context-Aware Constrained Reinforcement Learning Algorithm
 

---

**Input:** Initialize  $\varrho_1, \varrho_2, \varrho_3, \theta_0, \psi_0$ , and  $\{\omega_{k,0}, \phi_{k,0}\}_{k=1:K}$ .  
**for**  $i = 0, 1, \dots$  **do**

Sampling  $\varepsilon_i$  based on  $\pi_{\theta_i}$  and store it in the buffer.

**The CI Module:**

**for**  $t = Bi - B + 1, \dots, Bi$  **do**

Calculate  $E_{\psi_i}(z_t | \tau_t)$  and sample  $z_t \sim E_{\psi_i}(z_t | \tau_t)$ .

Replace  $s_t$  according to (2)

Calculate  $F_{\phi_{k,i}}(s_t, s_{t+1}) = V_{\phi_{k,i}}(s_{t+1}) - V_{\phi_{k,i}}(s_t)$ .

Reshape  $\{C'_k(s_t, a_t)\}_{k=1:K}$  by (3).

**The CRL Module:**

**The Critic Step:**

Estimate  $\hat{f}_{k,i}$  according to (9) and (8).

Set  $\omega_{k,i} \leftarrow \omega_{k,i-1}, \psi_{k,i} \leftarrow \psi_{k,i-1}, \phi_{k,i} \leftarrow \phi_{k,i-1}$ .

**for**  $t_{\text{cri}} = 1, \dots, T_{\text{cri}}$  **do**

Update  $\omega_{k,i}, \psi_{k,i}, \phi_{k,i}$  by (11), (16), (18), respectively.

Estimate  $\hat{g}_{k,i}$  according to (13) and (14).

**The Actor Step:**

Update the surrogate function  $\{\bar{f}_k(\theta_i)\}_{k=0,\dots,K}$  via (4).

Solve (5) if (5) is feasible. (*Objective update*)

Solve (6) if (5) is not feasible. (*Feasible update*)

Update policy parameters  $\theta_{i+1}$  according to (7).

---

If problem (5) turns out to be infeasible, the following feasible update problem is solved:

$$\bar{\theta}_i = \underset{\theta \in \Theta, y}{\operatorname{argmin}} \alpha \quad \text{s.t.} \quad \bar{f}_{k,i}(\theta) \leq \alpha, \forall k. \quad (6)$$

Please note that the surrogate problems (5) and (6) both belong to the convex quadratic problem, which can be easily solved by standard convex optimization algorithms, e.g. Lagrange-dual methods. Then, with  $\bar{\theta}_i$  given in one of the above two cases,  $\theta_i$  is updated according to

$$\theta_i = (1 - \mu_i)\theta_{i-1} + \mu_i\bar{\theta}_i. \quad (7)$$

where the step size  $\{\mu_i\}$  is a decreasing sequence satisfying Assumption 2 in section IV-B.

2) *The Critic Step for Estimating Function Values and Gradients:* The Critic step aims to calculate the estimated function values  $\{\hat{f}_{k,i+1}\}_{k=0,\dots,K}$  and the estimated gradients  $\{\hat{g}_{k,i+1}\}_{k=0,\dots,K}$  based on their historical values and the new observation set  $\varepsilon_i$ , and then uses them to construct  $\{\bar{f}_{k,i+1}(\theta)\}_{k=0,\dots,K}$  in the next iteration. First, we calculate a new estimation of function value using the sample average approximation (SAA) method as follows:

$$\tilde{f}_{k,i} = \hat{\mathbb{E}}_{\varepsilon_i}[C'_{k,t}], \forall k, \quad (8)$$

where  $\hat{\mathbb{E}}_{\varepsilon_i}$  denotes the sample average operation over the observation set  $\varepsilon_i$ . To reduce oscillations and accelerate convergence, we update  $\hat{f}_{k,i+1}$  by

$$\hat{f}_{k,i+1} = (1 - \eta_{i+1})\hat{f}_{k,i} + \eta_i\tilde{f}_{k,i}, \forall k, \quad (9)$$

where the step size  $\{\eta_i\}$  is a decreasing sequence satisfying Assumption 2 in section IV-B.

Then, for any  $\pi_{\theta_i}$ , there is a set of state-action value

functions (Q-functions)  $\{Q_k^{\pi_{\theta_i}}\}_{k=0,\dots,K}$  formulated as:

$$Q_k^{\pi_{\theta_i}}(s, a) = \mathbb{E}\left[\sum_{l=0}^{\infty} (\dot{C}'_{k,l} - f_{k,i}(\theta)) | s_0, a_0 = s, a\right].$$

Since it is unrealistic to obtain  $f_{k,i}(\theta)$  online, we replace it by  $\hat{f}_{k,i}$  and redefine a surrogate Q-function of  $Q_k^{\pi_{\theta_i}}, \forall k$ :

$$\hat{Q}_k^{\pi_{\theta_i}}(s, a) = \mathbb{E}\left[\sum_{l=0}^{\infty} (\dot{C}'_{k,l} - \hat{f}_{k,i}) | s_0, a_0 = s, a\right].$$

Considering the state space  $\mathcal{S}$  and the action space  $\mathcal{A}$  are continuous, a set of DNNs (Q-networks)  $\{Q_{\omega_{k,i}}\}_{k=0,\dots,K}$  is employed to parameterize  $\{\hat{Q}_k^{\pi_{\theta_i}}\}_{k=0,\dots,K}$ . The gap between the estimated Q-value  $Q_{\omega_{k,i}}(s, a)$  and the Q-value  $\hat{Q}_k^{\pi_{\theta_i}}(s, a)$  can be measured using the squared Bellman error:

$$\mathcal{B}_{k,i}(s_t, a_t, s_{t+1}) = |Q_{\omega_{k,i}}(s_t, a_t, s_{t+1}) - \mathcal{T}Q_{\omega_{k,i}}(s_t, a_t, s_{t+1})|^2, \forall k, \quad (10)$$

where  $\mathcal{T}$  is the Bellman operator defined as

$$\mathcal{T}Q_{\omega_{k,i}}(s_l, a_l) = \mathbb{E}\left[Q_{\omega_{k,i}}(s_{l+1}, a'_{l+1}) + \dot{C}'_{k,l}\right] - \hat{f}_{k,i}.$$

The Q-networks are optimized to minimize the mean-squared Bellman error using the classical TD-learning method [6]. Specifically, the new observation set  $\varepsilon_i$  is divided into  $T_{\text{cri}}$  ( $T_{\text{cri}} < B$ ) batches, where the observation index set of these batches are  $[\varepsilon_i^1, \dots, \varepsilon_i^{t_{\text{cri}}}, \dots, \varepsilon_i^{T_{\text{cri}}}]$ , and the following TD-updates are performed for  $T_{\text{cri}}$  times:

$$\omega_{k,i} \leftarrow \omega_{k,i} - v_i G_{k,i,t_{\text{cri}}}^{\mathcal{B}}, \forall k, t_{\text{cri}}, \quad (11)$$

where  $G_{k,i,t_{\text{cri}}}^{\mathcal{B}}$  is a stochastic gradient term given by

$$G_{k,i,t_{\text{cri}}}^{\mathcal{B}} = \sum_{t \in \varepsilon_i^{t_{\text{cri}}}} \left( Q_{\omega_{k,i}}(s_t, a_t) - \dot{C}'_{k,t} + \hat{f}_{k,i} - Q_{\omega_{k,i}}(s_{t+1}, a'_{t+1}) \right) \nabla_{\omega} Q_{\omega_{k,i}}(s_t, a_t), \forall k, \quad (12)$$

where the step size  $\{v_i\}$  is a decreasing sequence satisfying Assumption 2 in section IV-B.

Further, according to the policy gradient theorem [34]:

$$\nabla f_{k,i}(\theta) = \mathbb{E}\left[Q_k^{\pi_{\theta_i}}(s, a) \nabla_{\theta} \log \pi_{\theta_i}(a | s)\right], \forall k,$$

and following the SAA method, we calculate the new estimated gradient  $\tilde{g}_{k,i}$  by

$$\tilde{g}_{k,i} = \hat{\mathbb{E}}_{\varepsilon_i}\left[Q_{\omega_{k,i}}(s, a) \nabla_{\theta} \log \pi_{\theta_i}(a | s)\right], \forall k. \quad (13)$$

Finally, similar to (9),  $\hat{g}_{k,i}$  is updated according to

$$\hat{g}_{k,i+1} = (1 - \eta_{i+1})\hat{g}_{k,i} + \eta_i\tilde{g}_{k,i}, \forall k. \quad (14)$$

### C. The CI Module

1) *Context-aware Meta-learning:* Due to the potential variation of latent variables at each timeslot, the CI module estimates  $z_t$  through a  $\psi$ -parameterized encoder network  $E_{\psi}$  at each timeslot  $t$ . Specifically, we use  $E_{\psi}(z_t | \tau_t)$  to approximate the posterior of  $z_t$  and sample  $z_t$  from  $E_{\psi}(z_t | \tau_t)$ , where recall that  $\tau_t = \{\tilde{\tau}_{t'} = (s_{t'}, a_{t'}, s_{t'+1})\}_{t'=t-N+1:t}$ .



Note that this probabilistic modeling of  $z_t$  can enable CRL algorithms to explore more efficiently, due to the introduction of extra randomness [29]. Considering the encoder for a CMDP should be independent of the permutation of context tuples, its structure is designed as a product of some independent factors:

$$E_\psi(z_t|\tau_t) \propto \prod_{t'=t-N+1}^N e_\psi(z_{t'}|\tilde{\tau}_{t'}) = \mathcal{N}(E_\psi^u(\tau_t), E_\psi^\sigma(\tau_t)),$$

where  $e_\psi(z_t|\tilde{\tau}_{t'})$  represents the Gaussian distribution  $\mathcal{N}(e_{\psi_\mu}^u(\tilde{\tau}_{t'}), e_{\psi_\sigma}^\sigma(\tilde{\tau}_{t'}))$  with  $\psi \triangleq [\psi_\mu, \psi_\sigma]$ . Moreover,  $E_\psi^u(\tau_t)$  and  $E_\psi^\sigma(\tau_t)$  can be respectively given by

$$E_\psi^u(\tau_t) = E_\psi^\sigma(\tau_t) \cdot \prod_{t'=t-N+1}^t e_{\psi_\mu}^u(\tilde{\tau}_{t'})/e_{\psi_\sigma}^\sigma(\tilde{\tau}_{t'}),$$

$$E_\psi^\sigma(\tau_t) = \left( \prod_{t'=t-N+1}^t \frac{1}{e_{\psi_\sigma}^\sigma(\tilde{\tau}_{t'})} \right)^{-1}.$$

Now, we elaborate on how to optimize the encoder. Previous work [31] directly uses a  $z$ -parameterized DNN to fit the transition function and optimizes  $z$  to reconstruct to reconstruct trajectory  $\{s_0, a_0, s_1, a_1, \dots\}$ , which belongs to a model-based optimization method. However, this method incurs substantial additional training costs, as estimating the transition function is unnecessary in standard model-free Actor-Critic algorithms, and model-based approaches often yield significant errors in the learned transition function when the environment model is complex [35]. Considering that  $\hat{Q}_k^{\pi_\theta}$  is defined as the future expected average reward over the current policy and transition probability function  $P_T$ , it is clear that the optimization process of Q-networks involves learning  $P_T$  in a model-free manner. This motivates this paper to optimizes  $E_\psi(z|\tau)$  and Q-networks  $\{Q_{\omega_k}\}_{k=0,\dots,K}$  simultaneously, with the goal of enabling  $z$  to aid  $\{Q_{\omega_k}\}_{k=0,\dots,K}$  in reconstructing the Q-functions  $\{\hat{Q}_k^{\pi_\theta}\}_{k=0,\dots,K}$ , where more accurate  $z$  estimates lead to smaller reconstruction errors.

To facilitate joint training with the CRL module, the encoder network is updated once every  $B$  timeslots. Specifically, at the  $i$ -th iteration, we first define an optimal fitting variable  $O_i$  with  $O_i = 1$  representing the Q-networks  $\{Q_{\omega_{k,i}}\}_{k=0,\dots,K}$  achieves optimal reconstruction for the Q-functions  $\{\hat{Q}_k^{\pi_\theta}\}_{k=0,\dots,K}$ . Accordingly,  $P(O_i = 1|z_i)$  represents the probability that  $O_i = 1$  holds given  $z_i = \{z_t, Bi - N + 1 \leq t \leq Bi\}$ . Considering that the squared Bellman errors  $\mathcal{B}_{k,i}$  in (10) reflect the reconstruction error of Q-functions, we related it to  $P(O_i = 1|z_i)$  by

$$P(O_i = 1|z_i) \propto \exp\left(-\sum_{t=Bi-N+1}^{Bi} \sum_{k=1}^K \mathcal{B}_{k,i}(\dot{s}_t, a_t, \dot{s}_{t+1})\right),$$

Moreover,  $P(z_i|O_i = 1)$  represents the probability that  $z_i$  is the most effective for guiding the reconstruction of Q-functions during the  $i$ -th iteration. Following the mean-field variational Bayesian inference method [36], we use a variational distribution of product form  $q(z_i; \psi) = \prod_{t=Bi-N+1}^{Bi} E_\psi(z_t|\tau_t)$  to approximate  $P(z_i|O_i = 1)$ . This optimization objective is to minimize the Kullback-Leibler Divergence between  $q(z_i; \psi)$  and  $P(z_i|O_i = 1)$  as:

$$\begin{aligned} & \sum_{i=0}^{\infty} D_{\text{KL}}[q(z_i; \psi) || P(z_i|O_i = 1)] \\ &= \sum_{i=0}^{\infty} \mathbb{E}_{z_t \sim E_\psi} \left[ -\log \frac{P(O_i = 1|z_i) P(z_i)}{q(z_i; \psi) P(O_i = 1)} \right] \\ & \propto \mathbb{E}_{z_t \sim E_\psi} \left[ -\log P(O_i = 1|z_i) \right] + D_{\text{KL}}[q(z_i; \psi) || P(z_i)] \\ &= \underbrace{\sum_{i=0}^{\infty} \mathbb{E}_{z_t \sim E_\psi} \left[ \sum_{t=Bi-N+1}^{Bi} \sum_{k=1}^K \mathcal{B}_{k,i}(\dot{s}_t, a_t, \dot{s}_{t+1}) \right]}_{\mathcal{L}_{\text{meta}}^1(\psi)} \\ & \quad + \underbrace{\sum_{i=0}^{\infty} \sum_{t=Bi-N+1}^{Bi} D_{\text{KL}}[E_\psi(z_t|\tau_t) || P(z_t)]}_{\mathcal{L}_{\text{meta}}^2(\psi)}, \end{aligned} \quad (15)$$

We solve this by performing the following SGD for  $T_{\text{cri}}$  times at the  $i$ -th iteration:

$$\psi_i \leftarrow \psi_i - \nu_i \left( \sum_{k=1}^K G_{k,i,t_{\text{cri}}}^{\mathcal{L}^1} + G_{i,t_{\text{cri}}}^{\mathcal{L}^2} \right), \forall t_{\text{cri}}, \quad (16)$$

where  $G_{k,i,t_{\text{cri}}}^{\mathcal{L}^1}$  and  $G_{i,t_{\text{cri}}}^{\mathcal{L}^2}$  are stochastic gradients of  $\mathcal{L}_{\text{meta}}^1(\psi)$  and  $\mathcal{L}_{\text{meta}}^2(\psi)$ . The term  $G_{k,i,t_{\text{cri}}}^{\mathcal{L}^1}$  is given by

$$G_{k,i,t_{\text{cri}}}^{\mathcal{L}^1} = \sum_{t \in \varepsilon_i^{t_{\text{cri}}}} \left( Q_{\omega_{k,i}}(\dot{s}_t, a_t) - C'_{k,t} + \hat{f}_{k,i} - Q_{\omega_{k,i}}(\dot{s}_{t+1}, a'_{t+1}) \right) \nabla_{z_t} Q_{\omega_{k,i}}(\dot{s}_t, a_t) \cdot \nabla_{\psi} z_t$$

where denoting  $\xi_{t_{\text{cri}}}$  as a constant generated from Gaussian distribution  $\mathcal{N}(0, 1)$ , we have

$$\nabla_{\psi} z_t = \nabla_{\psi} E_\psi^u(\tau_t) + \xi_t \nabla_{\psi} E_\psi^\sigma(\tau_t).$$

Note that  $G_{k,i,t_{\text{cri}}}^{\mathcal{L}^1}$  can be calculated simultaneously with  $G_{k,i,t_{\text{cri}}}^{\mathcal{B}}$  in (12) simultaneously through the same backpropagations. Moreover, the stochastic gradient  $G_{i,t_{\text{cri}}}^{\mathcal{L}^2}$  is given by

$$G_{i,t_{\text{cri}}}^{\mathcal{L}^2} = \sum_{t \in \varepsilon_i^{t_{\text{cri}}}} E_\psi^u(\tau_t) \nabla_{\psi} E_\psi^u(\tau_t) - \frac{\nabla_{\psi} E_\psi^\sigma(\tau_t)}{2E_\psi^\sigma(\tau_t)}.$$

**2) Potential-based Reward-Reshaping:** The reward-reshaping functions in (3) are chosen to be  $F_{\phi_{k,i}}(\dot{s}_t, \dot{s}_{t+1}) = V_{\phi_{k,i}}(\dot{s}_{t+1}) - V_{\phi_{k,i}}(\dot{s}_t)$ ,  $k = 1, \dots, K$ , where  $V_{\phi_{k,i}}$  is a  $\phi_{k,i}$ -parameterized potential networks used to approximate the following optimal value function [37]:

$$V_k^{\pi_{\theta^*}}(\dot{s}) = \mathbb{E}_{a \sim \pi_{\theta^*}} [Q_k^{\pi_{\theta^*}}(\dot{s}, a)], \forall k, \quad (17)$$

where  $\theta^*$  is a KKT point of problem (1). Note that since the input space of  $V_k^{\pi_{\theta^*}}$  is much smaller than that of  $Q_k^{\pi_{\theta^*}}$ , it is also easier to be estimated and can serve as the prior representing the risk of packet dropout.

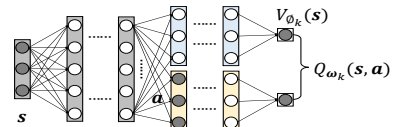


Figure 3. The framework of dual-head networks

Then, the potential networks  $\{V_{\phi_k}\}_{k=1,\dots,K}$  are also op-

timized with Q-networks  $\{Q_{\omega_k}\}_{k=1,\dots,K}$  simultaneously. To reduce computational costs, we integrate them into  $K$  dual-head networks shown in Fig. 3, whose shallow layers are shared for extracting features from  $\hat{s}_t$ . According to (17), we optimize  $\{V_{\phi_{k,i}}\}_{k=1,\dots,K}$  by performing the following SGD for  $T_{\text{cri}}$  times at the  $i$ -th iteration:

$$\phi_{k,i} \leftarrow \phi_{k,i} - v_i \sum_{t \in \varepsilon_i^{t_{\text{cri}}}} [\nabla \phi | V_{\phi_{k,i}}(\hat{s}_t) - \hat{V}_{k,t}|^2], \forall k, \quad (18)$$

where  $\hat{V}_{k,t} = \frac{1}{N_a} \sum_{n_a=1}^{N_a} Q_{\omega_{k,i}}(\hat{s}_t, \mathbf{a}_t^{n_a})$  is the SAA-based estimation of  $\mathbb{E}_{\mathbf{a} \sim \pi_{\theta}}[Q^{\pi_{\theta}}(\hat{s}, \mathbf{a})]$  with  $\{\mathbf{a}_t^{n_a}\}_{n_a=1:N_a}$  representing  $N_a$  actions sampled from  $\pi_{\theta}(\cdot | \hat{s})$ , and  $V_{k,i}$  is treated as a variable independent of  $\phi_{k,i}$  in the derivation operation.

#### IV. THEORETICAL ANALYSES OF ALGORITHM CONVERGENCE

To provide deeper insight into the CACRL algorithm, this section presents some theoretical analyses in an ideal case that CI module can accurately estimate  $\{z_t\}_{t=0,1,\dots}$  and  $V_k^{\pi_{\theta^*}}(\hat{s})$  through the encoder and potential networks. Specifically, we first prove that reward-reshaping does not change the optimal policy of problem (1). Then, based on some standard assumptions, we analyze the convergence of surrogate functions in the CRL module and prove that the CACRL can converge to a KKT point (up to a tolerable error) of problem (1).

##### A. Optimal Policy Invariance of the Reward-Reshaping

By performing (3), the reward-reshaping method transforms the original problem (1) into the following problem:

$$\min_{\theta \in \Theta} \dot{f}_0(\theta) \quad \text{s.t.} \dot{f}_k(\theta), k = 1, \dots, K, \quad (19)$$

where  $\{\dot{f}_k(\theta)\}_{k=0,\dots,K}$  are reshaped functions given by replacing  $\{C'_k\}_{k=1,\dots,K}$  in the definition of  $\{f_k(\theta)\}_{k=0,\dots,K}$  with  $\{\dot{C}'_k\}_{k=1,\dots,K}$ . By deriving the expression for the reshaped function  $\dot{f}_k(\theta)$ , we further obtain

$$\begin{aligned} \dot{f}_k(\theta) &= \lim_{T \rightarrow \infty} \frac{1}{T} \mathbb{E} \left[ \sum_{t=0}^{T-1} C'_k(s_t, \mathbf{a}_t) + F_{\phi_k}(\hat{s}_t, \hat{s}_{t+1}) \right], \\ &= \lim_{T \rightarrow \infty} \frac{1}{T} \mathbb{E} \left[ \sum_{t=0}^{T-1} C'_k(s_t, \mathbf{a}_t) + V_{\phi_k}(\hat{s}_{t+1}) - V_{\phi_k}(\hat{s}_t) \right], \\ &= \lim_{T \rightarrow \infty} \frac{1}{T} [V_{\phi_k}(\hat{s}_0) - V_{\phi_k}(\hat{s}_{T-1})] \\ &\quad + \lim_{T \rightarrow \infty} \frac{1}{T} \mathbb{E} \left[ \sum_{t=0}^{T-1} C'_k(s_t, \mathbf{a}_t) \right] \\ &= f_k(\theta), k. \end{aligned} \quad (20)$$

Therefore, we can conclude that the reward-reshaping method does not change the optimal policy of the problem (1).

##### B. Key Assumptions on Problem and Step Sizes

We first give some assumptions on the problem structure:

*Assumption 1. (Assumptions on the Problem Structure:)*

1) The state space  $\mathcal{S} \subseteq \mathbb{R}^{n_s}$ , the latent variable space  $\mathcal{Z} \subseteq \mathbb{R}^{n_z}$ , and the action space  $\mathcal{A} \subseteq \mathbb{R}^{n_a}$  are compact,

where  $n_s$ ,  $n_z$ , and  $n_a$  are some positive integers. The functions  $\{\dot{C}'_k\}_{k=0,\dots,K}$ , are bounded.

2) The policy  $\pi_{\theta}$  follows Lipschitz continuity over  $\theta \in \Theta$ , where the parameter spaces  $\Theta \subseteq \mathbb{R}^{n_{\theta}}$  is compact and convex.

3) The gradients of  $\dot{f}_k(\theta)$ ,  $\forall k$ , are uniformly bounded follow Lipschitz continuity over the parameter  $\theta \in \Theta$ .

4) There are constants  $\lambda > 0$  and  $\rho \in (0, 1)$  satisfying

$$\sup_{s \in \mathcal{S}} d_{\text{TV}}(P_S(\dot{s}_t | \dot{s}_0 = \dot{s}), \mathbf{P}_{\pi_{\theta}}(\dot{s}_t)) \leq \lambda \rho^t,$$

for all  $t = 0, 1, \dots$ , where  $P_S$  denotes the augmented state distribution,  $\mathbf{P}_{\pi_{\theta}}$  is the stationary case of  $P_S$  under policy  $\pi_{\theta}$ , and  $d_{\text{TV}}(\alpha, \beta) = \int_{\dot{s} \in \mathcal{S}} |\alpha(d\dot{s}) - \beta(d\dot{s})|$  indicates the total-variation distance between the probability measures  $\alpha$  and  $\beta$ .

Assumption 1-1) requires the augmented state space and action spaces be continuous. Assumption 1-2) can be easily satisfied as long as there is no gradient explosion during the training process. Assumption 1-3) holds based on the condition that the gradient of DNNs are bounded and satisfy Lipschitz continuity. Assumption 1-4) controls the bias caused by the Markovian noise in the observations by assuming the uniform ergodicity of the Markov chain generated by  $\pi_{\theta}$ , which is a standard requirement in [6], [34], [38].

Then, we lay down some assumptions about the choice of algorithm step sizes:

*Assumption 2. (Assumptions on step sizes:)*

The step-sizes  $\{\eta_i\}$ ,  $\{\mu_i\}$ , and  $\{v_i\}$  are deterministic and non-increasing, and satisfy:

- 1)  $\mu_i \rightarrow 0$ ,  $\sum_i \mu_i = \infty$ ,  $\sum_i (\mu_i)^2 < \infty$ ,
- 2)  $\eta_i \rightarrow 0$ ,  $\frac{1}{\eta_i} \leq O(i^{\varrho})$  for some  $\varrho \in (0, 1)$ ,  $\sum_i (\eta_i)^2 < \infty$ , and  $\lim_{i \rightarrow \infty} \mu_i \eta_i^{-1} = 0$ ,
- 3)  $v_i \rightarrow 0$ ,  $\sum_i v_i = \infty$ ,  $\sum_i (v_i)^2 < \infty$ .

A typical choice of step sizes  $\{\eta_i\}$ ,  $\{\mu_i\}$ , and  $\{v_i\}$  satisfying Assumption 2 is  $\mu_i = O(i^{-\varrho_1})$ ,  $\eta_i = O(i^{-\varrho_2})$ , and  $v_i = O(i^{-\varrho_3})$ , where  $\varrho_1, \varrho_2, \varrho_3 \in (0.5, 1)$  and  $\varrho_2 < \varrho_1$ .

##### C. Convergence Analyses

First, we provide the finite-time average estimation error of  $\hat{f}$  and  $\hat{g}$ , which reflects the convergence rate of surrogate functions in CSSCA method:

*Lemma 1. (Convergence rate of the Surrogate Functions:)*

The average estimation errors of  $\hat{f}$  and  $\hat{g}$  are given by

$$\begin{aligned} \epsilon_f(i) &\triangleq \frac{1}{1+i} \sum_{i'=0}^i \mathbb{E} \left[ (\hat{f}_{i'} - \dot{f}(\theta_{i'}))^2 \right] \leq O \left( \frac{1}{(1+i)\eta_{i+1}} \right) \\ &\quad + O \left( \frac{1}{1+i} \sum_{i'=0}^i (\mu_{i'} \log^2 i + \frac{\mu_{i'}^2}{\eta_{i'+1}^2} + \frac{\mu_{i'}^2}{\eta_{i'+1}} + \eta_{i'+1} \log i) \right), \\ \epsilon_g(i) &\triangleq \frac{1}{1+i} \sum_{i'=0}^i \mathbb{E} \left[ \|\hat{g}_{i'} - \nabla \dot{f}(\theta_{i'})\|_2^2 \right] \leq O \left( \frac{1}{(1+i)\eta_{i+1}} \right) \\ &\quad + O \left( \frac{1}{1+i} \sum_{i'=0}^i (\mu_{i'} \log^2 i + \frac{\mu_{i'}^2}{\eta_{i'+1}^2} + \frac{\mu_{i'}^2}{\eta_{i'+1}} + \eta_{i'+1}) \right) \\ &\quad + \epsilon_Q + \sqrt{\epsilon_f(i)}, \end{aligned}$$

where  $\epsilon_Q \triangleq O(\max_{\dot{s}, \mathbf{a}} |Q_{\omega_i}(\dot{s}, \mathbf{a}) - \hat{Q}^{\pi_{\theta_i}}(\dot{s}, \mathbf{a})|)$  represents the error magnitude of the estimated Q-values output Q-

networks. Suppose Assumptions 1 - 2 are satisfied, it is obtained that  $\lim_{i \rightarrow \infty} \epsilon_f(i) = 0$  and  $\lim_{i \rightarrow \infty} \epsilon_g(i) = \epsilon_Q$ .

*Proof:* Please refer to Appendix A for details. ■

It has been proven in [34] that the updates in (11) can reduce  $\epsilon_Q$  to 0 by increasing the interaction times  $B$  and the update times  $T_{\text{cri}}$  in each iteration, as long as the representational capacity of the Q-networks is sufficiently strong. Therefore, by choosing appropriate values for  $B$ ,  $T_{\text{cri}}$ , and the size of Q-networks, we can ensure that  $\epsilon_Q$  meets a practical tolerance standard. More intuitively, if we choose the typical step sizes mentioned above, use the fact that  $\frac{1}{1+i} \sum_{i'=0}^i (1+i')^{-\varrho} \leq (1+i')^{-\varrho} (1-\varrho)^{-1}$ , it can be obtained that

$$\epsilon_f(i) \leq O(i^{\varrho_1-1} + i^{-\varrho_1} \log i + i^{2\varrho_1-2\varrho_2})$$

$$\epsilon_g(i) \leq O(i^{\frac{\varrho_1-1}{2}} + i^{\frac{-\varrho_1}{2}} \log i + i^{\varrho_1-\varrho_2} + \epsilon_Q).$$

Moreover, we also demonstrate that the estimated value  $\hat{f}_{k,i}$  and estimated gradient  $\hat{g}_{k,i}$  for constructing surrogate functions satisfy the following asymptotic consistency:

*Lemma 2. (Asymptotic consistency of surrogate functions)* Suppose that Assumptions 1 and 2 are satisfied, we have

$$\lim_{t \rightarrow \infty} |\hat{f}_{k,i} - \dot{f}_{k,i}(\theta)| = 0, \forall k, \quad (21)$$

$$\lim_{t \rightarrow \infty} \|\hat{g}_{k,i} - \nabla \dot{f}_{k,i}(\theta_i)\|_2 \leq \epsilon_Q, \forall k, \quad (22)$$

where  $\epsilon_Q \triangleq O(\max_{\dot{s}, \mathbf{a}} |Q_{\omega_i}(\dot{s}, \mathbf{a}) - \hat{Q}^{\pi_{\theta_i}}(\dot{s}, \mathbf{a})|)$ .

*Proof:* Please refer to Appendix B for details. ■

Then, considering a subsequence  $\{\theta_{i_j}\}_{j=1}^{\infty}$  converging to a limiting point  $\theta^*$ , there exist converged surrogate functions

$$\lim_{j \rightarrow \infty} \bar{f}_{k,i_j}(\theta) = \hat{f}_k(\theta), \forall \theta \in \Theta, \forall k, \quad (23)$$

$$\text{where } |\hat{f}_k(\theta^*) - \dot{f}_k(\theta^*)| = 0, \quad (24)$$

$$\|\nabla \hat{f}_k(\theta^*) - \nabla \dot{f}_k(\theta^*)\|_2 = 0. \quad (25)$$

Finally, with section IV-A, Lemma 1, and Assumptions 1 - 2, we are ready to prove the main convergence theorem:

*Theorem 1. (Global Convergence of Algorithm 1:)*

Suppose Assumptions 1 - 2 are satisfied and the initial point  $\theta_0$  is feasible, i.e.,  $\max_{k \in \{1, \dots, K\}} f_k(\theta_0) \leq 0$ . Denote  $\{\theta_i\}_{i=1}^{\infty}$  as the iterates generated by the CRL module with a sufficiently small initial step size  $\mu_0$ . Then, every limiting point  $\theta^*$  of  $\{\theta_i\}_{i=1}^{\infty}$  satisfying the Slater condition satisfies KKT conditions up to an error  $\epsilon_Q$ , i.e.,

$$\|g_0(\theta^*) + \sum_k \lambda_k g_k(\theta^*)\|_2 \leq \epsilon_Q$$

$$f_k(\theta^*) \leq \epsilon_Q, k = 1, \dots, K,$$

$$\lambda_k f_k(\theta^*) \leq \epsilon_Q, k = 1, \dots, K,$$

where  $\epsilon_Q \rightarrow 0$  as  $B \rightarrow \infty$  and  $T_{\text{cri}} \rightarrow \infty$  for sufficiently large size of Q-networks.

*Proof:* The key challenges lie in the proof of Lemma 1 and 2. Once Lemma 1 and 2 are proved, Theorem 1 follows from the similar analyses in our previous work [39] and [6], and we omit it due to the space limit. ■

*Remark 2.* In practice, the pre-trained encoder network and potential networks unavoidably output imperfect estimates due to the limited number of updates, the finite representational capacity of DNNs, etc. However, the simulation results in the next section will demonstrate that these estimates, despite their errors, can still effectively capture the current traffic dynamics and packet dropout risks. With these estimates, the proposed CACRL is able to much better handle non-stationary XR data traffic with sparse delayed packet loss rewards, compared to standard CRL algorithms designed for general CMDPs and those incorporating gradient-based meta-learning methods. Moreover, the CRL module also contributes to the excellent performance of CACRL, due to its design for non-convex problems and strict theoretical convergence guarantees.

## V. SIMULATION SETUP

We consider a MU-MIMO system with one BS with  $M = 8$  transmitting antennas and  $K = 2 \sim 12$  single-antenna XR users. We adopt a geometry-based channel model  $\mathbf{h}_k = \sum_{l=1}^{N_p} \bar{\alpha}_{k,l} \mathbf{a}(\psi_{k,l})$ ,  $\forall k$  with  $N_p$  scattering path following the same setting in [6]. Specifically, the coefficient  $\bar{\alpha}_{k,l} \sim \mathcal{CN}(0, \bar{\sigma}_{k,l}^2)$  is Laplacian distributed, where  $\sum_{l=1}^{N_p} \bar{\sigma}_{k,l}^2 = g_k$ ,  $\bar{\sigma}_{k,l}^2$  follows an exponential distribution normalized such that  $\sum_{l=1}^{N_p} \bar{\sigma}_{k,l}^2 = g_k$ , and  $g_k$  represents the path gain of the  $k$ -th user. We uniformly generate the path gains  $g_k$ 's from -10 dB to 10 dB and set  $N_p = 4$  for each user.  $\mathbf{a}(\psi_{k,l})$  is the half-wavelength spaced uniform linear array (ULA) response vector, where  $\psi_{k,l}$  denotes the  $l$ -th angle of departure (AoD) with an angular spread  $\sigma_{AS} = 5$ . In addition, the bandwidth  $W = 10$  MHz, and the noise power density is -100 dBm/Hz.

We set the duration of one timeslot to  $\tau_0 = 1$  ms. At each timeslot  $t$ , we set packets arrive with probabilities  $P_k$  ranging from 0.2  $\sim$  0.8. The length  $b_{k,t}$  generating from a Poisson distribution  $P_{\text{poi}}(b_k = x) = \frac{(\lambda_k)^x}{x!} e^{-\lambda_k}$ , where  $\lambda_{k,t}$  randomly ranging from 5  $\sim$  20 Kbits. The allowed maximum packet dropout rate  $c_{k=1,2,\dots,K}$  are set to 10%. A similar packet arrival model and parameter settings are also adopted in [2], [40], and [41]. All CRL algorithms update their policies every 200 timeslots ( $B = 200$ ). In stationary scenarios, we assume that  $P_k$  and  $\lambda_k$  remain unchanged, while in non-stationary scenarios they are regenerated on average every  $E$  timeslots (we refer to  $E$  timeslots as one episode in the following). For the CACRL algorithm, we pre-train the CI module for 300 episodes,  $\zeta_k = 1, \forall k$ , and the step size parameters are chosen as  $\varrho_1 = 0.6, \varrho_2 = 0.7, \varrho_3 = 0.3$ . All simulation results below are averaged across 10 random seeds.

### A. Performance Analysis

1) *Performance in XR with Stationary Data Traffic:* We begin with testing algorithms in stationary XR scenarios. The number of users  $K = 4$ , and the parameters  $P_k$  and  $\lambda_k$  are ranging from [0.4, 0.6] and [10, 15] Kbits. Our baseline algorithms include two classical CDAC algorithms, CPO and PPO-Lag [15], and an advanced Actor-only algorithm, SCAOPO [6], introduced in Section I. All these baselines are standard CRL algorithms designed for stationary environments, with their policy networks taking only the observable state  $s$  as



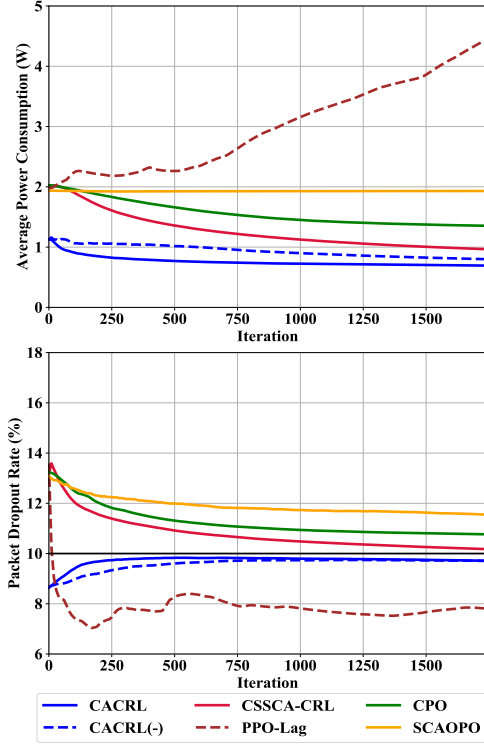


Figure 4. Convergence curves in scenario with stationary XR data traffic.

input. Moreover, we also simulate two variants of CACRL for ablation experiments: CSSCA-CRL and CACRL(-), where the former does not employ the CI module, and the latter only incorporates context-aware meta-learning method.

In Fig. 4, it can be seen that since the policy optimization methods in CPO and PPO-Lag are only suited for convex constrained problem, they are less effective than CACRL and its variants in satisfying packet dropout rate constraints and saving transmission power. Moreover, SCAOPO also struggles to satisfy the constraints due to the inaccurate Q-value estimation. Comparing CACRL(-) with CSSCA-CRL, we can see that the former converges faster, as its pre-trained encoder provides the CRL module with additional information about the environment dynamics. The results also show that CACRL converges faster than CACRL(-), highlighting the superiority of the reward-reshaping method.

#### 2) Performance in XR with Non-stationary Data Traffic:

Then, we evaluate algorithms in a more challenging XR scenarios with non-stationary data traffic. The number of users  $K = 4$ , and the parameters  $P_k$  and  $\lambda_k$  are also ranging from  $[0.4, 0.6]$  and  $[10, 15]$  Kbits. Since there are almost no existing CDAC algorithms for non-stationary environments apart from the MAML-CPO in [27], we chose MAML-CPO as a baseline for comparison with our algorithm. Note that MAML typically belongs to the gradient-based meta-learning methods introduced in Section I. Additionally, we simulated an algorithm that combines the MAML with the CRL module of CACRL, namely MAML-CSSCA-CRL. Note that MAML-CPO and MAML-CSSCA-CRL are also pre-trained for 300 episodes. Moreover, CACRL(-) and CSSCA-CRL are also simulated for ablation experiments.

Fig. 5 shows the convergence curves of the algorithms in a

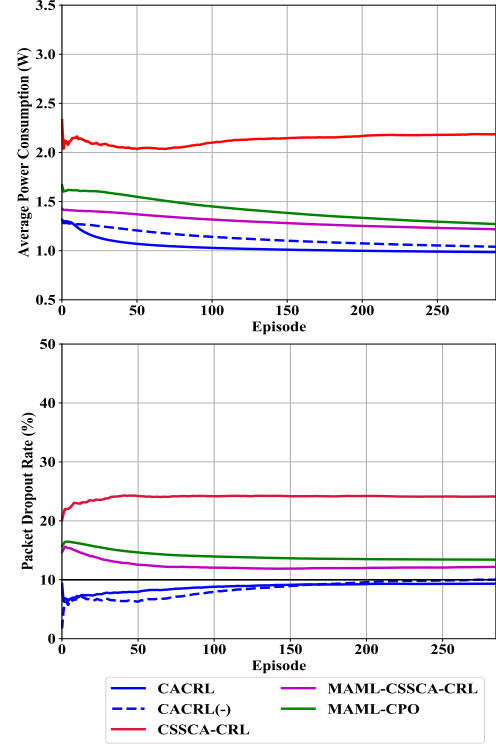


Figure 5. Convergence curves in scenario with non-stationary XR data traffic.

typical scenario with the duration of each episode  $E = 10B$  timeslots. In the ablation experiments, the proposed CACRL outperforms the CACRL(-) both in convergence speed and power consumption, further demonstrating the effectiveness of reward-reshaping. Additionally, it is evident that CSSCA-CRL performs poorly, highlighting the importance of designing CI module for CRL algorithms to handle the challenges posed by non-stationary XR data traffic. Regarding the comparative experiments, it is evident that although MAML CSSCA-CDAC also incorporates the meta-learning method MAML, it does not perform as well as CACRL and CACRL(-). This is primarily because MAML, as a gradient-based meta-learning approach, is less effective compared to context-based meta-learning methods in rapidly changing environments. Furthermore, it can be seen that the proposed CACRL algorithm greatly surpasses MAML-CPO due to its superior performance in both the CRL module and the CI module. For more details, we also tested MAML-CPO and MAML-CSSCA-CRL alongside the proposed CACRL in scenarios with the duration of each episode  $E = 2B, 5B, 10B, 20B$  timeslots, respectively. Fig. 6 indicates that under rapidly changing packet arrival dynamics, the MAML-CSSCA-CRL algorithm struggles to meet constraints and the MAML-CPO almost fails to work. In contrast, because CACRL is designed to prioritize satisfying constraints with the feasible update in (6) before reducing power consumption with the objective update in (5), it tends to learn a 'safe' policy, resulting in a packet dropout rate somewhat below the allowable limit. Although this may cause power consumption to be higher in scenarios with rapidly changing packet arrival dynamics compared to those with slower dynamics, it remains lower than that of the other two baselines in the same scenario due to its superior policy optimization method and advanced CI module.

Table I  
PERFORMANCE VERSUS THE PACKET SIZES

Algorithm	CADAC			MAML CSSCA-CRL			MAML CPO		
Size	Short	Medium	Large	Short	Medium	Large	Short	Medium	Large
Power Consumption (W)	0.76	0.99	1.36	0.95	1.22	2.06	1.14	1.27	2.86
Packet Dropout Rate (%)	9.19	9.34	10.56	9.94	12.20	12.64	12.45	13.41	18.35

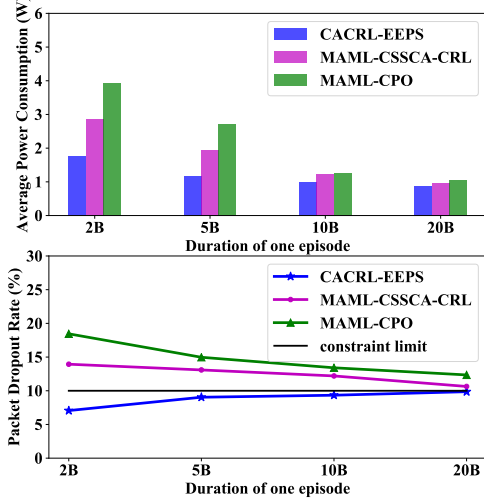


Figure 6. Performance versus different dynamic varying rates.

3) *Impact of Packet Sizes*: Moreover, we pre-train algorithms in scenarios with different packet sizes, and show their performance at the deployment stage in Tab. I. Specifically, in scenarios with packet sizes of “Short”, “Medium”, and “Large”,  $P_k$  ranges from  $[0.6, 0.8]$ ,  $[0.4, 0.6]$ , and  $[0.2, 0.4]$ , respectively, while  $\lambda_k$  ranges from  $[5, 10]$  Kbits,  $[10, 15]$  Kbits, and  $[15, 20]$  Kbits, respectively. Generally, scenarios with long packet sizes are more critical and challenging because larger packets indicate sparse feedback rewards, which can easily lead to algorithm convergence failures. It can be observed that in scenarios with large packets, the MAML-CSSCA-CRL algorithm requires relatively higher power consumption, and the performance of MAML-CPO deteriorates sharply to the extent that even with higher power consumption, it cannot provide the reliability needed to meet the packet loss constraints. In contrast, our algorithm maintains almost the same performance across all these scenarios, further demonstrating the effectiveness of the reward-shaping mechanism.

4) *Impact of Number of Users*: Finally, we also pre-train algorithms in scenarios with different numbers of users, where the parameters  $P_k$  and  $\lambda_k$  are ranging from  $[0.4, 0.6]$  and  $[10, 15]$  Kbits. Fig. 7 presents performance of algorithms in scenarios with different numbers of users. First, it can be seen that our algorithm uses less power resources compared to the other two baselines across various scenarios. Then, when it comes to guaranteeing QoS constraints, all algorithms perform better with fewer users but deteriorate as the number of users increases. This is because with more users, the EEPS problem becomes more non-convex and more complex packet arrival processes, leading to worse performance and slower convergence of algorithms. However, due to the the CSSCA-based policy optimization method, which is better suited for non-convex problems, and the advanced CI module, our algorithm still outperforms the other two baseline algorithms

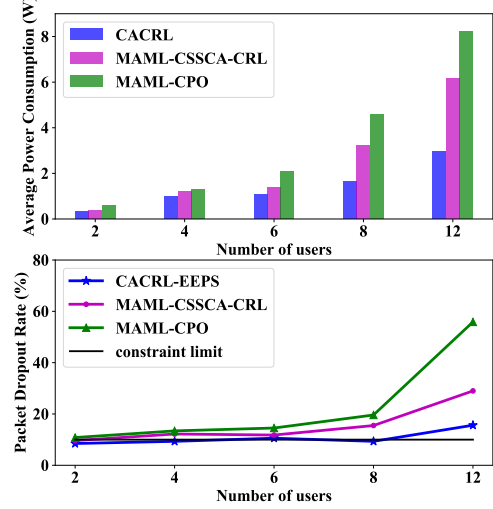


Figure 7. Performance versus the number of users.

even with a larger number of users.

## VI. CONCLUSION

This paper investigates a novel CACRL algorithm composed of a CRL module and a CI module, aiming at supporting XR transmission with minimal transmitted power resources. The CACRL formulates the EEPS task as a DP-CMDP, which appropriately capture its requirements and characteristics. In the CI module, we adopt the context-aware meta-learning method and the reward-resaping method to transform the original DP-CMDP to a general CMDP with immediate dense packet dropout rewards, enabling the CACRL algorithm to effectively handle non-stationary XR data traffic, even when packet dropout rewards are sparse and delayed. In the CRL module, we introduce a CSSCA-based policy optimization method, which can address non-convex stochastic constraints more effectively than conventional methods. Theoretical analysis is provided to offer deep insight into the algorithm’s convergence, and simulation results demonstrate that the proposed CACRL algorithm outperforms advanced baselines, making it highly promising for future XR transmission applications.

## APPENDIX A PROOF OF LEMMA 1

Since the analysis for  $\epsilon_f(i)$  and  $\epsilon_g(i)$  in Theorem 1 are similar, we only present the more intractable derivation of  $\epsilon_g(i)$  due to the space limit. We first define

$$\mathbf{b}_i = \hat{\mathbf{g}}_i - \nabla \dot{f}(\boldsymbol{\theta}_i),$$

$$\Upsilon(\varepsilon_{i+1}, \hat{\mathbf{g}}_i, \boldsymbol{\theta}_i, Q_{\omega_{i+1}}) = \langle \mathbf{b}_i, \tilde{\mathbf{g}}_{i+1} - \nabla \dot{f}(\boldsymbol{\theta}_i) \rangle,$$

where the subscript  $k$  is omitted to simplify notation. Then, according to (14), it can be derived that

$$\begin{aligned}
\|\mathbf{b}_{i+1}\|_2^2 &= \|\mathbf{b}_i + \nabla \dot{f}(\boldsymbol{\theta}_i) - \nabla \dot{f}(\boldsymbol{\theta}_{i+1}) + \eta_{i+1}(\tilde{\mathbf{g}}_{i+1} - \hat{\mathbf{g}}_i)\|_2^2 \\
&\leq \|\mathbf{b}_i\|_2^2 + 2\eta_{i+1}\mathbf{b}_i^\top (\tilde{\mathbf{g}}_{i+1} - \hat{\mathbf{g}}_i) + 2\|\nabla \dot{f}(\boldsymbol{\theta}_i) - \nabla \dot{f}(\boldsymbol{\theta}_{i+1})\|_2^2 \\
&\quad + 2\mathbf{b}_i^\top (\nabla \dot{f}(\boldsymbol{\theta}_i) - \nabla \dot{f}(\boldsymbol{\theta}_{i+1})) + 2\eta_{i+1}^2 \|\tilde{\mathbf{g}}_{i+1} - \hat{\mathbf{g}}_i\|_2^2 \\
&= (1 - 2\eta_{i+1})\|\mathbf{b}_i\|_2^2 + 2\eta_{i+1}\mathcal{R}(\varepsilon_{i+1}, \hat{\mathbf{g}}_i, \boldsymbol{\theta}_i, Q\boldsymbol{\omega}_{i+1}) \\
&\quad + 2\mathbf{b}_i^\top (\nabla \dot{f}(\boldsymbol{\theta}_i) - \nabla \dot{f}(\boldsymbol{\theta}_{i+1})) + 2\|\nabla \dot{f}(\boldsymbol{\theta}_i) - \nabla \dot{f}(\boldsymbol{\theta}_{i+1})\|_2^2 \\
&\quad + 2\eta_{i+1}^2 \|\tilde{\mathbf{g}}_{i+1} - \hat{\mathbf{g}}_i\|_2^2.
\end{aligned}$$

Rearranging, taking expectation, and taking summation on both sides, we obtain that

$$\begin{aligned}
&\frac{1}{1+i} \sum_{i'=0}^i \mathbb{E}[\|\mathbf{b}_{i'}\|_2^2] \\
&\leq \underbrace{\frac{1}{1+i} \sum_{i'=0}^i \frac{1}{2\eta_{i'+1}} \mathbb{E}[\|\mathbf{b}_{i'}\|_2^2 - \|\mathbf{b}_{i'+1}\|_2^2]}_{A_1(i)} \\
&\quad + \underbrace{\frac{1}{1+i} \sum_{i'=0}^i \frac{1}{\eta_{i'+1}} \mathbb{E}[\|\nabla \dot{f}(\boldsymbol{\theta}_{i'}) - \nabla \dot{f}(\boldsymbol{\theta}_{i'+1})\|_2^2]}_{A_2(i)} \\
&\quad + \underbrace{\frac{1}{1+i} \sum_{i'=0}^i \eta_{i'+1} \mathbb{E}[\|\tilde{\mathbf{g}}_{i'+1} - \hat{\mathbf{g}}_{i'}\|_2^2]}_{A_3(i)} \\
&\quad + \underbrace{\frac{1}{1+i} \sum_{i'=0}^i \mathbb{E}[\mathcal{R}(\varepsilon_{i'+1}, \hat{\mathbf{g}}_{i'}, \boldsymbol{\theta}_{i'}, Q\boldsymbol{\omega}_{i'+1})]}_{A_4(i)} \\
&\quad + \underbrace{\frac{1}{1+i} \sum_{i'=0}^i \frac{1}{\eta_{i'+1}} \mathbb{E}[\langle \mathbf{b}_{i'}, \nabla \dot{f}(\boldsymbol{\theta}_{i'}) - \nabla \dot{f}(\boldsymbol{\theta}_{i'+1}) \rangle]}_{A_5(i)},
\end{aligned} \tag{26}$$

For the first term  $A_1(i)$ ,

$$\begin{aligned}
A_1(i) &= \frac{1}{1+i} \sum_{i'=0}^i \frac{1}{2\eta_{i'+1}} \mathbb{E}[\|\mathbf{y}_{i'}\|_2^2 - \|\mathbf{y}_{i'+1}\|_2^2] \\
&= \frac{1}{1+i} \left( \sum_{i'=0}^i \left( \frac{1}{2\eta_{i'+1}} - \frac{1}{2\eta_{i'}} \right) \mathbb{E}[\|\mathbf{b}_{i'}\|_2^2] \right. \\
&\quad \left. + \frac{1}{2\eta_1} \mathbb{E}[\|\mathbf{b}_0\|_2^2] - \frac{1}{2\eta_{i+1}} \mathbb{E}[\|\mathbf{b}_{i+1}\|_2^2] \right) \\
&\leq \frac{1}{1+i} \left( \sum_{i'=0}^i \left( \frac{1}{2\eta_{i'+1}} - \frac{1}{2\eta_{i'}} \right) b_{\max} \right. \\
&\quad \left. + \frac{1}{2\eta_1} b_{\max} - \frac{1}{2\eta_{i+1}} b_{\min} \right) \\
&= O\left(\frac{1}{1+i} \frac{1}{\eta_{i+1}}\right),
\end{aligned} \tag{27}$$

where  $b_{\max}$  and  $b_{\min}$  are the maximum and minimum values of  $\mathbb{E}[\|\mathbf{b}_{i'}\|_2^2]$ ,  $\forall i'$ , respectively.

In terms of  $A_2(i)$  and  $A_3(i)$ , we respectively have that

$$\begin{aligned}
A_2(i) &= \frac{1}{1+i} \sum_{i'=0}^i \frac{1}{\eta_{i'+1}} \mathbb{E}[\|\nabla \dot{f}(\boldsymbol{\theta}_{i'}) - \nabla \dot{f}(\boldsymbol{\theta}_{i'+1})\|_2^2] \\
&\stackrel{a}{=} O\left(\frac{1}{1+i} \sum_{i'=0}^i \frac{\mu_{i'}^2}{\eta_{i'+1}}\right),
\end{aligned} \tag{28}$$

$$\begin{aligned}
A_3(i) &= \frac{1}{1+i} \sum_{i'=0}^i \eta_{i'+1} \mathbb{E}[\|\tilde{\mathbf{g}}_{i'+1} - \hat{\mathbf{g}}_{i'}\|_2^2] \\
&\stackrel{a}{=} O\left(\frac{1}{1+i} \sum_{i'=0}^i \eta_{i'+1}\right),
\end{aligned} \tag{29}$$

where (28)-a follows from the Lipschitz continuity of  $\nabla \dot{f}(\boldsymbol{\theta})$ , and (29)-a utilize the boundedness of  $\|\tilde{\mathbf{g}}_{i+1} - \hat{\mathbf{g}}_i\|_2^2$ .

For  $A_4(i)$ , we denote a gradient term

$$\nabla \hat{f}(\boldsymbol{\theta}) = \mathbb{E}[\hat{Q}^{\pi_{\boldsymbol{\theta}}}(\dot{\mathbf{s}}, \mathbf{a}) \nabla_{\boldsymbol{\theta}} \log \pi_{\boldsymbol{\theta}}(\mathbf{a} | \dot{\mathbf{s}})], \tag{30}$$

and further denote  $\mathcal{R}(\varepsilon_{i+1}, \hat{\mathbf{g}}_i, \boldsymbol{\theta}_i, \hat{Q}^{\pi_{\boldsymbol{\theta}_i}}) = \langle \mathbf{b}_i, \nabla \hat{f}(\boldsymbol{\theta}_i) - \nabla f(\boldsymbol{\theta}_i) \rangle$  and  $\mathcal{R}(\hat{\mathbf{g}}_i, \boldsymbol{\theta}_i) = \langle \mathbf{b}_i, \nabla \hat{f}(\boldsymbol{\theta}_i) - \nabla f(\boldsymbol{\theta}_i) \rangle = 0$ . Then, we derive that

$$\begin{aligned}
&\mathbb{E}[\mathcal{R}(\varepsilon_{i'+1}, \hat{\mathbf{g}}_{i'}, \boldsymbol{\theta}_{i'}, Q\boldsymbol{\omega}_{i'+1})] \\
&= \mathbb{E}[\mathcal{R}(\varepsilon_{i'+1}, \hat{\mathbf{g}}_{i'}, \boldsymbol{\theta}_{i'}, Q\boldsymbol{\omega}_{i'+1}) - \mathcal{R}(\varepsilon_{i'+1}, \hat{\mathbf{g}}_{i'}, \boldsymbol{\theta}_{i'}, \hat{Q}^{\pi_{\boldsymbol{\theta}_{i'+1}}})] \\
&\quad + \mathbb{E}[\mathcal{R}(\varepsilon_{i'+1}, \hat{\mathbf{g}}_{i'}, \boldsymbol{\theta}_{i'}, \hat{Q}^{\pi_{\boldsymbol{\theta}_{i'+1}}}) - \mathcal{R}(\hat{\mathbf{g}}_{i'}, \boldsymbol{\theta}_{i'})] \\
&\stackrel{a}{\leq} \left| \mathbb{E}[\mathcal{R}(\varepsilon_{i'+1}, \hat{\mathbf{g}}_{i'}, \boldsymbol{\theta}_{i'}, Q\boldsymbol{\omega}_{i'+1}) - \mathcal{R}(\varepsilon_{i'+1}, \hat{\mathbf{g}}_{i'}, \boldsymbol{\theta}_{i'}, \hat{Q}^{\pi_{\boldsymbol{\theta}_{i'+1}}})] \right| \\
&\quad + \left| \mathbb{E}[\mathcal{R}(\varepsilon_{i'+1}, \hat{\mathbf{g}}_{i'}, \boldsymbol{\theta}_{i'}, \hat{Q}^{\pi_{\boldsymbol{\theta}_{i'+1}}}) - \mathcal{R}(\hat{\mathbf{g}}_{i'}, \boldsymbol{\theta}_{i'})] \right|.
\end{aligned} \tag{31}$$

Denoting the first term of (31)-a as  $D_1(i')$ , we have

$$\begin{aligned}
D_1(i') &= O(\mathbb{E}[\|\tilde{\mathbf{g}}_{i'+1} - \nabla \hat{f}(\boldsymbol{\theta}_{i'+1})\|_2]) \\
&\stackrel{a}{\leq} \frac{1}{B} \sum_{j=B i'+1}^{B i'+B} O(\|P_S(\dot{\mathbf{s}}_j) - \mathbf{P}_{\pi_{\boldsymbol{\theta}_{i'+1}}}(\dot{\mathbf{s}}_j)\|_{\text{TV}} \\
&\quad + |\mathbb{E}[Q\boldsymbol{\omega}_{i'+1}(\dot{\mathbf{s}}, \mathbf{a})] - \hat{Q}^{\pi_{\boldsymbol{\theta}_{i'+1}}}(\dot{\mathbf{s}}, \mathbf{a})|)
\end{aligned} \tag{32}$$

where (32)-a is derived according to the definitions of  $\tilde{\mathbf{g}}_{i'+1}$  and  $\nabla \hat{f}(\boldsymbol{\theta}_{i'+1})$  and the triangle inequality. By denoting an auxiliary trajectory  $\{\dot{\mathbf{s}}_{j-\kappa_i}, \tilde{\mathbf{a}}_{j-\kappa_i}, \dot{\mathbf{s}}_{j-\kappa_i+1}, \tilde{\mathbf{a}}_{j-\kappa_i+1}, \dots, \dot{\mathbf{s}}_j\}$  obtained by the fixed policy  $\pi_{\boldsymbol{\theta}_{i'+1}}$  from the initial state  $\dot{\mathbf{s}}_{j-\kappa_i} = \dot{\mathbf{s}}_{j-\kappa_i}$ , the first term of (32) can be derived as

$$\begin{aligned}
&O(\|P_S(\dot{\mathbf{s}}_j) - \mathbf{P}_{\pi_{\boldsymbol{\theta}_{i'+1}}}(\dot{\mathbf{s}}_j)\|_{\text{TV}}) \\
&\stackrel{a}{\leq} O(\|P_S(\dot{\mathbf{s}}_j) - P_S(\dot{\mathbf{s}}_{j-\kappa_i})\|_{\text{TV}} \\
&\quad + \|P_S(\dot{\mathbf{s}}_{j-\kappa_i}) - \mathbf{P}_{\pi_{\boldsymbol{\theta}_{i'+1}}}(\dot{\mathbf{s}}_j)\|_{\text{TV}}).
\end{aligned} \tag{33}$$

Following the similar tricks as (23)-(26) in [6], we have

$$\|P_S(\dot{\mathbf{s}}_j) - P_S(\dot{\mathbf{s}}_{j-\kappa_i})\|_{\text{TV}} \leq O(\kappa_i \sum_{l=j-\kappa_i}^j \mu_{[l/B]}). \tag{34}$$

According to Assumption 1-4), it is obtained that

$$\|P_S(\dot{\mathbf{s}}_{j-\kappa_i}) - \mathbf{P}_{\pi_{\boldsymbol{\theta}_{i'+1}}}(\dot{\mathbf{s}}_j)\|_{\text{TV}} = O(\rho^{\kappa_i}). \tag{35}$$

Denoting the second term of (32)-a as  $D_2(i)$ , we have

$$\begin{aligned} D_2(i') &= \mathbb{E} \left[ \left\| \nabla \hat{f}(\boldsymbol{\theta}_{i'} + 1) - \nabla \hat{f}(\boldsymbol{\theta}_{i'}) \right\|_2 \right] \\ &= O(\mathbb{E}[\|\hat{f}_{i'} - \hat{f}(\boldsymbol{\theta}_{i'})\|]). \end{aligned} \quad (36)$$

Therefore, combining (32)-(36) and setting  $O(\rho^{\kappa_i}) = O(\frac{1}{i})$ , i.e.,  $\kappa_i = O(\log i)$ , we can obtain that

$$\begin{aligned} A_4(i) &= O\left(\frac{1}{1+i} \sum_{i'=0}^i \mathbb{E}[\|\hat{f}_{i'} - \hat{f}(\boldsymbol{\theta}_{i'})\|]\right) \\ &\quad + \frac{1}{1+i} \sum_{i'=0}^i \left(\mu_{i'} \log^2 i + \frac{1}{i} + \epsilon_{\text{cri}}(i')\right) \\ &\stackrel{a}{\leq} O\left(\sqrt{\frac{1}{1+i} \sum_{i'=0}^i \mathbb{E}[\|\hat{f}_{i'} - \hat{f}(\boldsymbol{\theta}_{i'})\|^2]}\right) \\ &\quad + \frac{1}{1+i} \sum_{i'=0}^i \left(\mu_{i'} \log^2 i + \frac{1}{i} + \epsilon_Q(i')\right) \end{aligned} \quad (37)$$

For  $A_5(t)$ , we have

$$\begin{aligned} A_5(i) &= \frac{1}{1+i} \sum_{i'=0}^i \frac{1}{\eta_{i'+1}} \mathbb{E} \left[ \mathbf{b}_{i'}^\top (\nabla \hat{f}(\boldsymbol{\theta}_{i'}) - \nabla \hat{f}(\boldsymbol{\theta}_{i'+1})) \right] \\ &\stackrel{a}{\leq} \sqrt{\frac{1}{1+i} \sum_{i'=0}^i \mathbb{E}[\|\mathbf{b}_{i'}\|_2^2]} \sqrt{\frac{1}{1+i} \sum_{i'=0}^i \frac{(\nabla \hat{f}(\boldsymbol{\theta}_{i'}) - \nabla \hat{f}(\boldsymbol{\theta}_{i'+1}))^2}{\eta_{i'+1}^2}} \\ &\stackrel{b}{=} O\left(\sqrt{B(i)} \sqrt{\frac{1}{1+i} \sum_{i'=0}^i \frac{\mu_{i'}^2}{\eta_{i'+1}^2}}\right), \end{aligned} \quad (38)$$

where we define  $B(i) \triangleq \frac{1}{1+i} \sum_{i'=0}^i \mathbb{E}[\|\mathbf{b}_{i'}\|_2^2]$ . Please note that (38)-a follows from the Cauchy-Schwarz inequality, and (38)-b is because of the Lipschitz continuity of  $\nabla \hat{f}(\boldsymbol{\theta})$  and the update rule  $\boldsymbol{\theta}_{i'} = \boldsymbol{\theta}_{i'-1} + \eta_{i'}(\bar{\boldsymbol{\theta}}_{i'} - \boldsymbol{\theta}_{i'-1})$ .

Combining equations (27)-(38) and defining

$$\begin{aligned} C(i) &= \frac{1}{1+i} \sum_{i'=0}^i \frac{\mu_{i'}^2}{\eta_{i'+1}^2}, \\ A(i) &= A_1(i) + A_2(i) + A_3(i) + A_4(i). \end{aligned}$$

we have

$$\begin{aligned} B(i) &= O\left(\sqrt{B(i)} \sqrt{C(i)} + A(i)\right) \\ &\leq c_1 \sqrt{B(i)} \sqrt{C(i)} + O(A(i)), \end{aligned}$$

where  $c_0 > 0$  is some positive constant. Then, it is obtained

$$\begin{aligned} \left(\sqrt{B(i)} - \frac{c_0}{2} \sqrt{C(i)}\right)^2 &\leq \frac{c_0^2}{4} C(i) + O(A(i)) \\ \sqrt{B(i)} - \frac{c_0}{2} \sqrt{C(i)} &\leq \frac{c_0}{2} \sqrt{C(i)} + O(A(i)) \\ \sqrt{B(i)} &\leq c_0 \sqrt{C(i)} + O(A(i)) \\ B(i) &= O(C(i) + A(i)). \end{aligned} \quad (39)$$

This completes the proof.

## APPENDIX B PROOF OF LEMMA 2

Since the asymptotic consistency analyses for function values and gradients are similar, we will only present the latter. We first construct two auxiliary policy gradient estimates  $\nabla_{\boldsymbol{\theta}} \hat{f}_k(\boldsymbol{\theta}_i)$  and  $\hat{\mathbf{g}}_{k,i}$ . Specifically,  $\nabla_{\boldsymbol{\theta}} \hat{f}_k(\boldsymbol{\theta})$  is defined by

$$\nabla_{\boldsymbol{\theta}} \hat{f}_k(\boldsymbol{\theta}_i) = \mathbb{E}_{\sigma_{\pi_{\boldsymbol{\theta}_i}}} \left[ \hat{Q}_k^{\pi_{\boldsymbol{\theta}_i}}(\dot{s}, \mathbf{a}) \nabla_{\boldsymbol{\theta}} \log \pi_{\boldsymbol{\theta}_i}(\mathbf{a} | \dot{s}) \right], \forall k. \quad (40)$$

and  $\hat{\mathbf{g}}_{k,i}$  is obtained by

$$\hat{\mathbf{g}}_{k,i+1} = (1 - \eta_{i+1}) \hat{\mathbf{g}}_{k,i} + \eta_i \tilde{\mathbf{g}}_{k,i}, \forall k, i, \quad (41)$$

$$\tilde{\mathbf{g}}_{k,i} = \hat{\mathbb{E}}_{\varepsilon_i} \left[ \hat{Q}_k^{\pi_{\boldsymbol{\theta}_i}}(\dot{s}, \mathbf{a}) \nabla_{\boldsymbol{\theta}} \log \pi_{\boldsymbol{\theta}_i}(\mathbf{a} | \dot{s}) \right], \forall k, i. \quad (42)$$

Then, the asymptotic consistency of gradients can be decomposed into the following three steps:

$$\text{Step1 : } \lim_{t \rightarrow \infty} \|\nabla_{\boldsymbol{\theta}} \hat{f}_k(\boldsymbol{\theta}_i) - \nabla_{\boldsymbol{\theta}} \dot{f}_k(\boldsymbol{\theta}_i)\|_2 = 0, \quad (43)$$

$$\text{Step2 : } \lim_{t \rightarrow \infty} \|\hat{\mathbf{g}}_{k,i} - \nabla_{\boldsymbol{\theta}} \dot{f}_k(\boldsymbol{\theta}_i)\|_2 = 0, \quad (44)$$

$$\text{Step3 : } \lim_{t \rightarrow \infty} \|\hat{\mathbf{g}}_{k,i} - \tilde{\mathbf{g}}_{k,i}\|_2 = \epsilon_Q. \quad (45)$$

According to the definitions of  $\nabla_{\boldsymbol{\theta}} \hat{f}_k(\boldsymbol{\theta}_i)$ ,  $\nabla_{\boldsymbol{\theta}} \dot{f}_k(\boldsymbol{\theta}_i)$ ,  $\hat{\mathbf{g}}_{k,i}$ , and  $\tilde{\mathbf{g}}_{k,i}$ , it's easy to obtain that

$$\|\nabla_{\boldsymbol{\theta}} \hat{f}_k(\boldsymbol{\theta}_i) - \nabla_{\boldsymbol{\theta}} \dot{f}_k(\boldsymbol{\theta}_i)\|_2 = O(\|\hat{f}_{k,i} - \dot{f}_k(\boldsymbol{\theta}_i)\|_2),$$

$$\|\hat{\mathbf{g}}_{k,i} - \tilde{\mathbf{g}}_{k,i}\|_2 = O(\|Q_{\omega_{k,i}}(\dot{s}, \mathbf{a}) - \hat{Q}_k^{\pi_{\boldsymbol{\theta}_i}}(\dot{s}, \mathbf{a})\|_2) = \epsilon_Q.$$

Therefore, Step 1 holds as long as the asymptotic consistency of the function values holds, and Step 3 clearly holds.

In the following, we focus on proving the Step 2 in (44). This proof relies on a technical lemma [42, Lemma 1], which is restated below for completeness.

**Lemma 3.** Let  $(\Omega, \mathcal{G}, \mathbb{P})$  denote a probability space and let  $\{\mathcal{G}_t\}$  denote an increasing sequence of  $\sigma$ -field contained in  $\mathcal{G}$ . Let  $\{z^t\}$ ,  $\{w^t\}$  be sequences of  $\mathcal{G}_t$ -measurable random vectors satisfying the relations

$$w^{t+1} = \prod_{\mathcal{W}} (w^t + \alpha_t (\varrho^t - w^t)) \quad (46)$$

$$\mathbb{E}[\varrho^t | \mathcal{G}_t] = z^t + o^t$$

where  $\alpha_t \geq 0$  and the set  $\mathcal{W}$  is convex and closed,  $\prod_{\mathcal{W}}(\cdot)$  denotes projection on  $\mathcal{W}$ . Let

- (a) all accumulation points of  $\{w^t\}$  belong to  $\mathcal{W}$  w.p.l.,
  - (b) there is a constant  $C$  such that  $\mathbb{E}[\|\varrho^t\|_2 | \mathcal{G}_t] \leq C$ ,  $\forall t \geq 0$ ,
  - (c)  $\sum_{t=0}^{\infty} \mathbb{E}[(\alpha_t)^2 + \alpha_t \|\varrho^t\|] < \infty$
  - (d)  $\sum_{t=0}^{\infty} \alpha_t = \infty$ , and (e)  $\|z^{t+1} - z^t\|/\alpha_t \rightarrow 0$  w.p.l.,
- Then  $z^t - w^t \rightarrow 0$  w.p.1.

Since the step size  $\{\alpha_t\}$  follows Assumption 2, and  $\dot{C}_i, \forall i$  is bounded, it's easy to prove that the conditions (a), (b), and (d) in the Lemma above are satisfied. Now, we are ready to prove the technical condition (c).

Recalling the definition of  $\tilde{\mathbf{g}}_{k,i}$  and  $\nabla_{\boldsymbol{\theta}} \dot{f}_k(\boldsymbol{\theta}_i)$ , we obtain

the stochastic policy gradient error:

$$\begin{aligned} \|o^t\|_2 &= \|\tilde{g}_{k,i} - \nabla_{\theta} \hat{f}_k(\theta_i)\|_2 \\ &= \frac{1}{B} \sum_{j=Bt'+1}^{Bt'+B} O(\|P_S(\dot{s}_j) - \mathbf{P}_{\pi_{\theta_{t'+1}}}(\dot{s}_j)\|_{TV}). \end{aligned} \quad (47)$$

According to (32)-(34) in Appendix A of our manuscript and Assumption 2, it's easy to prove that condition (c) is held. Moreover, for the condition (e), we have

$$\begin{aligned} \|\nabla_{\theta} \hat{f}_i(\theta_{t+1}) - \nabla_{\theta} \hat{f}_i(\theta_t)\|_2 \\ = O(\|\theta_{t+1} - \theta_t\|_2 + \|\mathbf{P}_{\pi_{\theta_{t+1}}} - \mathbf{P}_{\pi_{\theta_t}}\|_{TV}) = O(\beta_t) \end{aligned} \quad (48)$$

It can be seen from Assumption 2 that technical condition (e) is also satisfied. This completes the proof of Step 2.

## REFERENCES

- [1] F. Alriksson, D. H. Kang, C. Phillips, J. L. Pradas, and A. Zaidi, "Xr and 5g: Extended reality at scale with time-critical communication," *Ericsson Technology Review*, vol. 2021, no. 8, pp. 2–13, 2021.
- [2] X. Zhao, Y.-J. A. Zhang, M. Wang, X. Chen, and Y. Li, "Online multi-user scheduling for xr transmissions with hard-latency constraint: Performance analysis and practical design," *IEEE Trans. Commun.*, 2024.
- [3] B. Chang, L. Zhang, L. Li, G. Zhao, and Z. Chen, "Optimizing resource allocation in urllc for real-time wireless control systems," *IEEE Trans. Veh. Technol.*, vol. 68, no. 9, pp. 8916–8927, 2019.
- [4] Z. Wei, Y. Cai, D. W. K. Ng, and J. Yuan, "Energy-efficient radio resource management," *Wiley 5G Ref: The Essential 5G Reference Online*, pp. 1–23, 2019.
- [5] R. Ruby, S. Zhong, D. W. K. Ng, K. Wu, and V. C. Leung, "Enhanced energy-efficient downlink resource allocation in green non-orthogonal multiple access systems," *Computer Communications*, vol. 139, pp. 78–90, 2019.
- [6] C. Tian, A. Liu, G. Huang, and W. Luo, "Successive convex approximation based off-policy optimization for constrained reinforcement learning," *IEEE Trans. Signal Process.*, vol. 70, pp. 1609–1624, 2022.
- [7] R. A. Berry and R. G. Gallager, "Communication over fading channels with delay constraints," *IEEE Trans. Inf. Theory*, vol. 48, no. 5, pp. 1135–1149, 2002.
- [8] Y. Mao, J. Zhang, S. H. Song, and K. B. Letaief, "Stochastic joint radio and computational resource management for multi-user mobile-edge computing systems," *IEEE Trans. Wireless Commun.*, vol. 16, no. 9, pp. 5994–6009, 2017.
- [9] S. Shakkottai and R. Srikant, "Scheduling real-time traffic with deadlines over a wireless channel," in *Proc. 2nd ACM international workshop on Wireless mobile multimedia*, 1999, pp. 35–42.
- [10] W. Chen, M. J. Neely, and U. Mitra, "Energy efficient scheduling with individual packet delay constraints: Offline and online results," in *Proc IEEE Int. Conf. Comput. Commun.*, 2007, pp. 1136–1144.
- [11] M. Khojastepour and A. Sabharwal, "Delay-constrained scheduling: power efficiency, filter design, and bounds," in *Proc IEEE Int. Conf. Comput. Commun.*, vol. 3, 2004, pp. 1938–1949 vol.3.
- [12] I. Fawaz, M. Sarkiss, and P. Ciblat, "Optimal resource scheduling for energy harvesting communications under strict delay constraint," in *Proc IEEE Int. Conf. Commun.*, 2018, pp. 1–6.
- [13] M. Sulaiman, M. Ahmadi, M. A. Salahuddin, R. Boutaba, and A. Saleh, "Generalizable resource scaling of 5G slices using constrained reinforcement learning," in *Proc. NOMS IEEE/IFIP Netw. Operations Manage. Symp.* IEEE, 2023, pp. 1–9.
- [14] K. Arulkumaran, M. P. Deisenroth, M. Brundage, and A. A. Bharath, "Deep reinforcement learning: A brief survey," *IEEE Trans. Signal Process.*, vol. 34, no. 6, pp. 26–38, 2017.
- [15] J. Achiam and D. Amodei, "Benchmarking safe exploration in deep reinforcement learning," 2019.
- [16] S. Khodadadian, T. T. Doan, J. Romberg, and S. T. Maguluri, "Finite sample analysis of two-time-scale natural actor-critic algorithm," *IEEE Trans. Automat. Contr.*, 2022.
- [17] D. Ding, K. Zhang, T. Basar, and M. Jovanovic, "Natural policy gradient primal-dual method for constrained markov decision processes," *Advances in Neural Information Processing Systems*, vol. 33, pp. 8378–8390, 2020.
- [18] D. Ding, C.-Y. Wei, K. Zhang, and A. Ribeiro, "Last-iterate convergent policy gradient primal-dual methods for constrained mdps," *Advances in Neural Information Processing Systems*, vol. 36, 2024.
- [19] D. Ding, X. Wei, Z. Yang, Z. Wang, and M. Jovanovic, "Provably efficient safe exploration via primal-dual policy optimization," in *International Conference on Artificial Intelligence and Statistics*. PMLR, 2021, pp. 3304–3312.
- [20] J. Achiam, D. Held, A. Tamar, and P. Abbeel, "Constrained policy optimization," in *ICML*. PMLR, 2017, pp. 22–31.
- [21] T.-Y. Yang, J. Rosca, K. Narasimhan, and P. J. Ramadge, "Projection-based constrained policy optimization," *arXiv preprint arXiv:2010.03152*, 2020.
- [22] Y. Zhang, Q. Vuong, and K. Ross, "First order constrained optimization in policy space," *Adv. Neural Inf. Process. Syst.*, vol. 33, pp. 15338–15349, 2020.
- [23] S. Paternain, L. Chamon, M. Calvo-Fullana, and A. Ribeiro, "Constrained reinforcement learning has zero duality gap," in *Advances in Neural Information Processing Systems*, H. Wallach, H. Larochelle, A. Beygelzimer, F. d'Alché-Buc, E. Fox, and R. Garnett, Eds., vol. 32. Curran Associates, Inc., 2019.
- [24] H. Hu, G. Huang, X. Li, and S. Song, "Meta-reinforcement learning with dynamic adaptiveness distillation," *IEEE Trans. Neural Netw. Learn. Syst.*, vol. 34, no. 3, pp. 1454–1464, 2021.
- [25] W. Wu, J. Dong, Y. Sun, and F. R. Yu, "Heterogeneous markov decision process model for joint resource allocation and task scheduling in network slicing enabled internet of vehicles," *IEEE Wireless Communications Letters*, vol. 11, no. 6, pp. 1118–1122, 2022.
- [26] C. Finn, P. Abbeel, and S. Levine, "Model-agnostic meta-learning for fast adaptation of deep networks," in *International conference on machine learning*. PMLR, 2017, pp. 1126–1135.
- [27] M. Cho and C. Sun, "Constrained meta-reinforcement learning for adaptable safety guarantee with differentiable convex programming," in *Proceedings of the AAAI Conference on Artificial Intelligence*, vol. 38, no. 19, 2024, pp. 20975–20983.
- [28] A. Nichol, J. Achiam, and J. Schulman, "On first-order meta-learning algorithms," *arXiv preprint arXiv:1803.02999*, 2018.
- [29] K. Rakelly, A. Zhou, C. Finn, S. Levine, and D. Quillen, "Efficient off-policy meta-reinforcement learning via probabilistic context variables," in *International conference on machine learning*. PMLR, 2019, pp. 5331–5340.
- [30] P. Jiang, S. Song, and G. Huang, "Exploration with task information for meta reinforcement learning," *IEEE Trans. Neural Netw. Learn. Syst.*, vol. 34, no. 8, pp. 4033–4046, 2021.
- [31] A. Xie, J. Harrison, and C. Finn, "Deep reinforcement learning amidst continual structured non-stationarity," in *International Conference on Machine Learning*. PMLR, 2021, pp. 11393–11403.
- [32] R. Zakhour and S. V. Hanly, "Base station cooperation on the downlink: Large system analysis," *IEEE Trans. Inf. Theory*, vol. 58, no. 4, pp. 2079–2106, 2012.
- [33] R. S. Sutton and A. G. Barto, *Reinforcement learning: An introduction*. MIT press, 2018.
- [34] P. Xu and Q. Gu, "A finite-time analysis of Q-learning with neural network function approximation," in *ICML*, 2020, pp. 10555–10565.
- [35] Q. Huang, "Model-based or model-free, a review of approaches in reinforcement learning," in *2020 International Conference on Computing and Data Science (CDS)*, 2020, pp. 219–221.
- [36] W. Han and Y. Yang, "Statistical inference in mean-field variational bayes," *arXiv preprint arXiv:1911.01525*, 2019.
- [37] H. Zou, T. Ren, D. Yan, H. Su, and J. Zhu, "Reward shaping via meta-learning," *arXiv preprint arXiv:1901.09330*, 2019.
- [38] S. Qiu, Z. Yang, J. Ye, and Z. Wang, "On finite-time convergence of actor-critic algorithm," *IEEE J. Sel. Areas Inf. Theory*, vol. 2, no. 2, pp. 652–664, 2021.
- [39] A. Liu, R. Yang, T. Q. S. Quek, and M.-J. Zhao, "Two-stage stochastic optimization via primal-dual decomposition and deep unrolling," *IEEE Trans. Signal Process.*, vol. 69, pp. 3000–3015, 2021.
- [40] I. Fawaz, M. Sarkiss, and P. Ciblat, "Optimal resource scheduling for energy harvesting communications under strict delay constraint," in *2018 IEEE International Conference on Communications (ICC)*, 2018, pp. 1–6.
- [41] A. T. Z. Kasgari and W. Saad, "Model-free ultra reliable low latency communication (urllc): A deep reinforcement learning framework," in *ICC 2019-2019 IEEE International Conference on Communications (ICC)*. IEEE, 2019, pp. 1–6.
- [42] A. Ruszczyński, "Feasible direction methods for stochastic programming problems," *Mathematical Programming*, vol. 19, no. 1, pp. 220–229, 1980.